Long-lived particles in the FASER and ATLAS detectors

Lotta van Broekhoven

Radboud University
Institute for Mathematics, Astrophysics and Particle Physics
Supervisor: Susanne Westhoff

4 Juli 2025

Acknowledgements

I wish to express my sincere gratitude to all those who provided me assistance while writing this thesis. I want to express my deepest gratitude to my supervisor Dr. Susanne Westhoff for her invaluable guidance throughout the course of this project, and for her willingness to answer all my questions.

Secondly, I want to acknowledge all the support of my parents while writing this thesis. I would also like to thank my partner for keeping me motivated and providing me with support during periods of writing-related challenges.

Contents

1 Introduction

In order to be able to test the Standard Model and other theories of physics, high precision experiments are needed. One of these experiments is ATLAS. The ATLAS detector is designed for multi-purpose detection, consisting of six different detecting subsystems. All these systems are located around one of the LHC interaction points. This results in more than a billion particle interactions within the ATLAS detector every second [1]. However, it can be hard to distinguish the different processes and to determine of which process the particles are a result. However, the ATLAS detector is not the only detector located near the ATLAS interaction point. FASER also detects particles produced at the LHC interaction point, albeit 480 meters away. Also, it is located along the beam collision axis, instead of around the interaction point, like the ATLAS detector.

In this research, the possibilities of finding sibling pairs of particles in both the FASER and ATLAS detectors will be discussed. The question that I will look into in this thesis is whether it is useful to link the FASER and ATLAS detectors. If this is possible, this could significantly reduce the background on the signal processes in FASER. As discussed, it can be hard to exactly determine which process resulted in the particles that are found by the ATLAS detector. However, if a similar event were to occur within the FASER detector as in the ATLAS detector, the event in the FASER detector could be used as a trigger for the ATLAS detector. This could significantly reduce the background of the process.

Here the model that will be used for the creation of this particle pair will be a dark matter benchmark model. This model is specifically chosen so that it is possible to create a particle pair where either of the two particles decays within the FASER and ATLAS detectors. In order to achieve this, the particles will need to be light, to travel in the forwards direction; be long-lived, to travel all the way to the FASER detector without decaying; and a pair has to be created. For this model, both a scalar singlet and a vector boson singlet will be added to the Standard Model.

In sections 2 and 3 the current Standard Model will be discussed, as well as how to extend the Standard Model. Here, also the dark matter benchmark model that is used in this thesis will be discussed. Section 4 contains relevant information on the detectors which will be used. Especially the geometry of the detectors will be of importance here. How the event simulations were performed and the parameters that play a role here are discussed in section 5. From these simulations the data sample was extracted for the data analysis to find particle pairs in both detectors. The results of this data analysis of the simulated data are shown in section 6 and discussed in section 7. Here the found results are also scaled up to meet the predicted luminosity of LHC run 4, in order to make realistic predictions.

2 The Standard Model and extensions thereof

Currently, the best way of describing the elementary particles and their interactions is through the Standard Model. These elementary particles make up all the matter that we can see around us. These particles fall into two categories: the quarks and the leptons. The quarks and the leptons come in what is called 3 generations. The first generation contains the lightest particles. These first generation particles make up the stable matter within the universe. Matter that is made up of particles from higher generations will decay into lighter generations. These elementary particles can in turn form mesons, made up of two quarks. Mesons will play an important role in this thesis, mainly the B meson. Next to this, the Standard Model is also able to describe electromagnetism, the strong force and the weak force. These three forces are carried by so-called bosons. The strong force is carried by the gluon, the weak force by the W and Z bosons, while electromagnetism is carried by the photon.

Many aspects of the Standard Model have been well tested by experiments. However, there are still shortcomings within the Standard Model. The Standard Model as we know it does not explain how gravity is mediated. Neither can it explain the disproportion between matter and anti-matter. But the most important shortcoming for this thesis is that the Standard Model is not able to describe dark matter. Only about 5% of the content of the universe is made up of matter which can be described through the Standard Model. Around 27% of the universe is estimated to be made up of dark matter [2].

In order to determine how dark matter can be described as an extension of the Standard Model, first, the Standard Model itself has to be described.

2.1 The Standard Model

For the description of the Standard Model, symmetries play a highly important role. Particle interactions will remain invariant under symmetry transformations under which they are charged. These symmetries can be described through the use of groups. The Standard Model respects the local gauge symmetry group $SU(3)_C \times SU(2)_L \times U(1)_Y$. The $SU(3)_C$ group represents the strong interactions, $SU(2)_L$ represents the weak interactions, and $U(1)_Y$ the hypercharge interactions. This means that the Standard Model interactions will remain invariant under any of these transformations. Here, the role of these symmetries is shown by discussing the description of electromagnetism by a Lagrangian. It is important to understand the importance of the symmetries in order to discuss possible extensions of the Standard Model.

Starting from the Dirac Lagrangian

$$\mathcal{L}(x) = i\bar{\psi}(x)\gamma^\mu\partial_\mu\psi(x) - m\bar{\psi}(x)\psi(x), \tag{1}$$

where m is the mass of the fermion, γ^μ represents the gamma matrix and $\bar{\psi} =$

$\psi \dagger \gamma^0$. When applying a local U(1) gauge transformation $\psi(x) \to e^{i\alpha(x)}\psi(x)$, the kinetic term of this Lagrangian leads to

$$i\bar{\psi}(x)\gamma^\mu\partial_\mu\psi(x) \to i\bar{\psi}(x)\gamma^\mu\partial_\mu\psi(x) - \bar{\psi}(x)\gamma^\mu\psi(x)\partial_\mu\alpha(x). \tag{2}$$

Here, the last term is generally not equal to 0, meaning that this is not locally invariant. In order to fix the addition of this extra term, the covariant derivative D_μ is introduced. The covariant derivative will transform such that

$$D_\mu\psi(x) \to D'_\mu\psi'(x) = e^{i\alpha(x)}D_\mu\psi(x). \tag{3}$$

This means that both $D_\mu\psi(x)$ and $\psi(x)$ will transform similarly under local gauge transformations. This can be assured by choosing a new vector field $A_\mu(x)$

$$D_\mu \equiv \partial_\mu + igA_\mu(x) \quad A_\mu(x) \to A'_\mu(x) = A_\mu(x) - \frac{1}{g}\partial_\mu\alpha(x). \tag{4}$$

Here g represents the gauge coupling, and the second transformation describes the electromagnetic gauge transformation.

So now the transformation of the covariant derivative can be shown as

$$\begin{aligned} D'_\mu\psi'(x) &= (\partial_\mu + ig(A_\mu(x) - \frac{1}{g}\partial_\mu\alpha(x)))e^{i\alpha(x)}\psi(x) \\ &= e^{i\alpha(x)}(\partial_\mu + i\partial_\mu\alpha(x) + igA_\mu(x) - i\partial_\mu\alpha(x))\psi(x) \\ &= e^{i\alpha(x)}D_\mu\psi(x). \end{aligned} \tag{5}$$

Thus, this means that the Dirac Lagrangian with the covariant derivative D_μ is now invariant under the local U(1) gauge transformation. Now, a gauge-invariant kinetic term still has to be added for the A_μ field. In order to achieve this, the term $-\frac{1}{4}F_{\mu\nu}(x)F^{\mu\nu}(x)$ is added to the Lagrangian. In this term $F_{\mu\nu}(x)$ is the gauge-invariant field tensor, $F_{\mu\nu} = \partial_\mu A_\nu - \partial_\nu A_\mu$.

Now, this locally invariant Lagrangian describes the electromagnetic interactions between matter fermions as being mediated by the photon.

$$\mathcal{L}_{em} = i\bar{\psi}(x)\gamma^\mu D_\mu\psi(x) - m\bar{\psi}(x)\psi(x) - \frac{1}{4}F_{\mu\nu}(x)F^{\mu\nu}(x) \tag{6}$$

2.2 Electroweak symmetry breaking

The mass of the particles also has to be able to be described by the Standard Model. However, simply adding mass terms of the form $m^2A_\mu A^\mu$ is not allowed. This is due to the symmetries discussed above. A fermionic mass term would not be gauge invariant under $SU(2)_L \times U(1)_Y$. These groups represent a chiral gauge theory, where different chiral states transform differently. The mass term

$m\bar{\psi}\psi = m(\bar{\psi}_R\psi_L + \bar{\psi}_L\psi_R$ would break this gauge invariance. In order to be able to add mass terms to the Lagrangian, the mass terms have to be generated, without changing the symmetries of the particles. This can be achieved through spontaneous symmetry breaking. The ground state is not a singlet of the symmetry group, so choosing one of the ground states as the physical vacuum can break the symmetry.

The most minimal way of achieving spontaneous symmetry breaking in the Standard Model is by adding a complex scalar field ϕ to the Lagrangian. This will be an $SU(2)_L$ doublet with weak isospin I = 1/2 and hypercharge Y = 1. The most general form of the Lagrangian is

$$\mathcal{L} = -\frac{1}{4}F_{\mu\nu}F^{\mu\nu} + (D_\mu\phi)^\dagger(D^\mu\phi) - V(\phi) \quad \text{where} \quad V(\phi) = \mu^2\phi^\dagger\phi + \lambda|\phi^4|. \quad (7)$$

Here, $\mu^2 < 0$ and $\lambda > 0$. Through this choice of μ and λ, the potential does not represent a parabola; rather, it acquires a ring of minima in the complex plane, of which one is shown in figure 1.

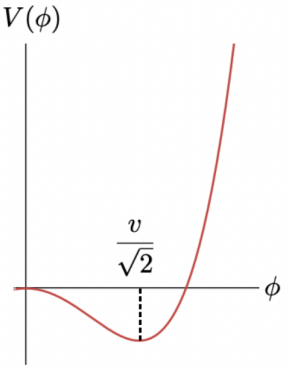

Figure 1: This is the shape of the Higgs potential for $V(\phi) = \mu^2\phi^\dagger\phi + \lambda|\phi^4|$, with $\mu^2 < 0$ and $\lambda > 0$.

From figure 1 it can be seen that at $\phi = 0$ the potential has a local maximum, while there is a ring of minima located at $v/\sqrt{2}$. Since there is now this ring of minima surrounding the local maximum at $\phi = 0$, $\phi = 0$ is no longer a suitable ground state. Rather, one of the minima of the ring should be the ground state. This ground state can be chosen such that $\langle\phi\rangle = v/\sqrt{2}$. In this ground state, the Higgs doublet thus becomes

$$\langle\phi\rangle = \frac{1}{\sqrt{2}}\begin{pmatrix}0\\v\end{pmatrix} \quad \text{where} \quad v = \left(\frac{\mu^2}{\lambda}\right)^{\frac{1}{2}}. \quad (8)$$

Here, v represents the vacuum expectation value (vev) of the theory. Now, we can re-parametrize ϕ and when switching to the unitary gauge, the Higgs field becomes

$$\phi(x) = \frac{1}{\sqrt{2}} \begin{pmatrix} 0 \\ v + h(x) \end{pmatrix}, \tag{9}$$

where $h(x)$ is the physical Higgs boson field. Now, for the covariant derivative acting on the field we find

$$D_\mu \phi = \left(\partial_\mu + \frac{i}{2}(g\vec{\sigma} \cdot \vec{W}_\mu + g' B_\mu) \right) \frac{1}{\sqrt{2}} \begin{pmatrix} 0 \\ v + h \end{pmatrix}, \tag{10}$$

where $\vec{\sigma}$ denotes the Pauli spin matrices, $\vec{W}_\mu$ represents the components of the W_μ field and B_μ also a new scalar field. Next to this it is also found that

$$-V(\phi) = \mu^2 h^2 - \lambda v h^3 - \frac{\lambda}{4} h^4 + \frac{1}{4} \lambda v^4. \tag{11}$$

Using this expression of the covariant derivative and the field on the Lagrangian from equation 7, the mass terms follow from the gauge-kinetic term $D_\mu \phi D^\mu \phi$. For the Z and W bosons the masses that are found are

$$m_W^2 = \frac{1}{4} v^2 g^2 \quad m_Z^2 = \frac{1}{4} v^2 (g^2 + g'^2) = m_W^2 / \cos\theta_W \quad m_A^2 = 0 \quad v = 246\text{GeV}. \tag{12}$$

2.3 Standard Model extensions

Now it is possible to discuss extensions of the Standard Model. In order to make extensions, it is important that the current structure of the Standard Model remains untouched. Here, one-particle extensions of the Standard Model will be discussed, since these extensions are what will be used later on in this thesis.

One way of extending the Standard Model is by introducing new particles which do not interact through the forces which are described by the Standard Model, thus these new particles will be uncharged under electromagnetism, the strong force and the weak force. These kinds of extensions ensure that the Standard Model remains untouched. Since these particles transform as singlets under the $SU(3)_C \times SU(2)_L \times U(1)_Y$, these kinds of one particle extensions will be called a 'singlet'. Three kinds of singlets can be added: a fermion, a gauge boson or a scalar particle.

2.3.1 Fermion singlet

In order to add a fermion singlet particle to the Standard Model, an extra Lagrangian term has to be added which describes the new interaction. Since

this new added neutrino N is invariant under all $SU(3)_C \times SU(2)_L \times U(1)_Y$ transformations, it is called sterile. This Lagrangian term is described as

$$\mathcal{L} = -Y_\nu \bar{L}\tilde{\phi}N_R + h.c. \tag{13}$$

Thus, through this portal, it is now possible for a right-handed neutrino to couple to the Standard Model. Hence, why this portal is often called a 'neutrino portal'.

2.3.2 Vector boson singlet

A new vector boson singlet can also be added to the Standard Model. The field to which this new vector boson can couple is the hypercharge field $B_{\mu\nu}$. It is only possible for the new vector boson to couple to this field, and not to the gluons G^A_μ or to the weak gauge bosons W^i_μ. This is because the $U(1)_Y$ symmetry is an abelian symmetry, while $SU(2)_L$ and $SU(3)_C$ are not. However, if the symmetries are not abelian, the field strength tensor is not invariant under the transformations. For the case where the symmetry is abelian, thus the $U(1)_Y$ case, the field strength tensor $B_{\mu\nu}$ will remain invariant under the transformations. The added Lagrangian term can thus be described as

$$\mathcal{L} = -\frac{\epsilon}{2\cos\theta_W} B_{\mu\nu} X^{\mu\nu}. \tag{14}$$

Here, X_μ is the new field belonging to the added vector boson singlet. This mixing is called kinetic mixing, where the ϵ parameter dictates the amount of mixing between the B and X fields. This is also the term similar to what I will add for generating the dark photon interactions.

2.3.3 Scalar singlet

The last portal that will be discussed is the portal to add a scalar singlet particle ϕ_D to the Standard Model. This coupling is only possible to the Higgs sector, hence why this portal is called the 'Higgs portal'. It is allowed to add terms to the Higgs sector, since the Higgs field combination $\phi^\dagger\phi$ is gauge invariant. This allows for the following Higgs potential

$$\mathcal{L} = -\mu^2|\Phi_{SM}|^2 - \mu_S^2|\Phi_D|^2 - \alpha|\Phi_{SM}|^2|\Phi_D|^2 - \beta|\Phi_{SM}|^2\Phi_D. \tag{15}$$

Here, α and β are new couplings, and the new mass term of the introduced scalar singlet, which is parametrized by μ and μ_S. These new terms will eventually lead to scalar mixing between the Standard Model Higgs and the newly introduced scalar singlet. Through this mixing, the new scalar singlet will pick up all the couplings of the Standard Model Higgs boson, with an extra scaling term. This Higgs portal will also be used in this thesis to introduce the new dark scalar particle.

So, now the importance of the symmetries within the Standard Model and how these symmetries affect the possible one-particle extension of the Standard Model has been discussed. Now it is possible to describe the dark matter benchmark model that will be used for this research.

3 The dark photon model

In order to find particle pairs in both the ATLAS and FASER detectors, the particle model first has to be discussed. This benchmark model of course has to be suited for the problem at hand. As stated in the introduction, the model needs to meet the following properties. First, the particles which are created need to be light, in order for them to be able to travel in the far-forwards direction. Next to this, the particles also need to be long-lived. This is needed since the FASER detector is located 480 meters away from the ATLAS interaction point. Lastly, the creation of two particles is needed, since one needs to be able to decay within the ATLAS detector, and one within the FASER detector.

The model that is able to fulfil these wishes includes adding a $U(1)_D$ symmetry to the Standard Model. This extension of the Standard Model results in a new vector boson singlet [3]. In this thesis, this new vector boson will be called the Dark Photon. In other literature, it can also be known as the Dark-Z [3]. The new $U(1)_D$ fields can interact with the Standard Model through kinetic mixing between the $U(1)_D$ and the $U(1)_Y$ fields of the Standard Model hypercharge gauge boson. The way that this mixing occurs is by adding new terms to the Standard Model Lagrangian. A new kinetic term for the $U(1)_D$ boson, and a mixing term are added. This added term can be found in Lagrangian 16 [3]. This Lagrangian with the added kinetic mixing term allows for the mixing between the $U(1)_D$ and the $U(1)_Y$ fields.

$$\mathcal{L} = -\frac{1}{4}\hat{B}_{\mu\nu}\hat{B}^{\mu\nu} - \frac{1}{4}\hat{Z}_{D,\mu\nu}\hat{Z}_D^{\mu\nu} + \frac{1}{2}\frac{\epsilon}{\cos\theta_W}\hat{B}_{\mu\nu}\hat{Z}_D^{\mu\nu} \tag{16}$$

Here, Z_D represents the new dark photon field. The fields are hatted, denoting that the fields are interaction eigenstates. The last term represents the kinetic mixing between the dark sector and the Standard Model. The ϵ is the kinetic mixing parameter, which governs how strong the mixing is between the dark sector and the Standard Model, where $\epsilon \sim 10^{-17} - 10^{-2}$ [3]. The $\cos\theta_W$ term represents the Weinberg angle. The fields are written as

$$\hat{B}_{\mu\nu} = \partial_\mu \hat{B}_\nu - \partial_\nu \hat{B}_\mu \quad \hat{Z}_{D,\mu\nu} = \partial_\mu \hat{Z}_{D,\nu} - \partial_\nu \hat{Z}_{D,\mu}. \tag{17}$$

First, the mixing term in the Lagrangian has to vanish, in order to get a proper Lagrangian without the mixing term. This is done by applying a shift on the B field [4]. The shift that is performed on the fields is to the first order in ϵ.

$$\begin{pmatrix} Z_D \\ B \end{pmatrix} = \begin{pmatrix} 1 & 0 \\ \frac{-\epsilon}{\cos\theta_W} & 1 \end{pmatrix} \begin{pmatrix} \hat{Z}_D \\ \hat{B} \end{pmatrix} \tag{18}$$

Thus, the shifted fields can be expressed as

$$\begin{aligned} \hat{Z}_D &= Z_D \\ \hat{B} &= \frac{\epsilon}{\cos\theta_W} Z_D + B. \end{aligned} \tag{19}$$

As can be seen from these expressions of the shifted fields, the dark photon field remains the same before and after the diagonalization, it does not pick up a B field component. However, the B field does pick up a dark photon component, which is proportional to ϵ.

Using these expressions for the fields on the Lagrangian from equation 16 will remove the mixing term from the Lagrangian. This is due to the B field now also containing a dark photon component. The Lagrangian thus becomes

$$\mathcal{L}_{gauge} = -\frac{1}{4} Z_{D,\mu\nu} Z_D^{\mu\nu} - \frac{1}{4} B_{\mu\nu} B^{\mu\nu}. \tag{20}$$

3.1 Mass mixing

From equation 19 it can thus be seen that the B field picks up a dark photon component. When applying electroweak symmetry breaking, this extra component will also have an effect on the Z boson and on the photon A.

$$\begin{pmatrix} A \\ Z \end{pmatrix} = \begin{pmatrix} \cos\theta_W & \sin\theta_W \\ -\sin\theta_W & \cos\theta_W \end{pmatrix} \begin{pmatrix} B \\ W^3 \end{pmatrix} \tag{21}$$

This matrix shows the relation between the B field and the third component of the W gauge field with respect to the photon and Z boson. When applying the diagonalized B field from equation 19 on the electroweak symmetry breaking, the new diagonalized fields become [4]

$$\begin{aligned} A &= \hat{A} - \epsilon Z_D \\ Z &= \hat{Z} + \epsilon \tan\theta_W Z_D \\ Z_D &= \hat{Z}_D. \end{aligned} \tag{22}$$

Where the hatted fields are the fields before the shift.

The mass term of the dark photons comes from additional terms added to the Higgs potential, namely

$$\mathcal{L} \supset (D_\mu \Phi_D)^\dagger (D^\mu \Phi_D), \tag{23}$$

where the covariant derivative is $D_\mu = \partial_\mu - \frac{i}{2} g_D Z_{D\mu}$ and the field $\Phi_D = \frac{1}{\sqrt{2}}(s + w)$. Here s represents the dark scalar field before diagonalization of the mass matrix, so not yet a mass eigenstate, and w is the vacuum expectation value (vev) for the dark scalar. g_D denotes the dark sector gauge coupling.

Putting this into the kinetic part of the Lagrangian gives the following mass term for the dark photon.

$$\mathcal{L} \supset \frac{1}{8} g_D^2 Z_{D\mu} Z_D^{\mu} w^2 \tag{24}$$

Thus, the dark sector part leads to a mass term of the form $\frac{1}{2} m_{Z_D}^2 \hat{Z}_{D\mu} \hat{Z}_D^{\mu}$, where $m_{Z_D} = \frac{1}{2} g_D w$. The Standard Model term from the Lagrangian leads to the mass of the Z boson, again of the form $\frac{1}{2} m_Z^2 \hat{Z}_{\mu} \hat{Z}^{\mu}$. However, since these fields also need to be diagonalized following equation 21, the Z fields now also have a Z_D contribution. This means that there is now mixing in the mass terms, and they are no longer diagonalized. The matrix that describes this mixing is given by

$$\mathcal{M}^2 = m_Z^2 \begin{pmatrix} 1 & -\epsilon \tan\theta_W \\ -\epsilon \tan\theta_W & \delta^2 + \epsilon^2 \tan^2\theta_W \end{pmatrix}, \tag{25}$$

where $\delta^2 = \frac{m_{Z_D}^2}{m_Z^2}$, in the basis of (Z, Z_D). Diagonalizing the matrix from equation 25 and the fields will give the mass eigenstates of the fields.

After diagonalization, the new fields can be described as a mixing of the old fields, namely

$$\begin{pmatrix} \tilde{Z} \\ \tilde{Z}_D \end{pmatrix} = \begin{pmatrix} \hat{Z}\cos\theta_D + \hat{Z}_D \sin\theta_D \\ -\hat{Z}\sin\theta_D + \hat{Z}_D \cos\theta_D \end{pmatrix}. \tag{26}$$

Here, the fields with a tilde indicate the fields after the diagonalization of the mass matrix. From here on forward, the tildes will be omitted, and the fields will always be the mass eigenstates. The mixing angle θ_d I found is given by the following expression, also in accordance with [5].

$$\tan\theta_d = \frac{-\left(1 - \delta^2 - \epsilon^2 \tan\theta_W^2\right) - \sqrt{\left(1 - \delta^2 - \epsilon^2 \tan\theta_W^2\right)^2 + 4\epsilon^2 \tan\theta_W^2}}{2\epsilon \tan\theta_W}. \tag{27}$$

The eigenvalues of the matrix lead to the new mass eigenstates, namely

$$m_{Z,Z_D}^2 = \frac{1}{2}\left(1 + \delta^2 + \epsilon^2 \tan^2\theta_W \pm \sqrt{\left(1 + \delta^2 + \epsilon^2 \tan^2\theta_W\right)^2 - 4\delta^2}\right). \tag{28}$$

Now, for $\delta << 1$ and $\epsilon << 1$ these masses of the fields after mixing result in [5]

$$\hat{m}_{Z_D}^2 \approx m_{Z_D}^2 (1 - \epsilon^2 \tan^2\theta_W) \quad \hat{m}_Z^2 \approx m_Z^2 (1 + \epsilon^2 \tan^2\theta_W). \tag{29}$$

The value for $\delta << 1$ can be assumed since the dark photon mass (~ 0.35 GeV) will be much lower than the mass of the Z boson (91 GeV [6]).

3.2 Dark scalar

Next to introducing the dark photon, another particle is added to our model. This particle will ensure that two dark photons will be created, as needed for the signature. The introduction of this new scalar, the dark scalar, leads to additional terms in the Lagrangian [7]. The new Higgs sector Lagrangian thus becomes

$$\mathcal{L} = (D_\mu \Phi_{SM})^\dagger (D^\mu \Phi_{SM}) + (D_\mu \Phi_D)^\dagger (D^\mu \Phi_D) + V_0. \tag{30}$$

Where the first two terms represent the kinetic part of the Higgs sector, and the V_0 term denotes the now altered Higgs potential. The covariant derivative of the Standard Model is given as $D_\mu = \partial_\mu - igI_W^a W_\mu^a + ig' \frac{Y_W}{2} B_\mu$, and the derivative acting on the dark scalar fields is given as $D_\mu = \partial_\mu - \frac{i}{2} g_D Z_{D\mu}$. In this covariant derivative, the g_D represents the dark sector gauge coupling. The last term, the potential, contains the following terms

$$V_0 = -\mu^2 |\Phi_{SM}|^2 - \mu_S^2 |\Phi_D|^2 - \lambda |\Phi_{SM}|^4 - \lambda_D |\Phi_D|^4 - \beta |\Phi_{SM}|^2 \Phi_D. \tag{31}$$

In this potential, μ and λ are the parameters from the Standard Model Higgs sector. The μ_S and λ_D denote the parameters belonging to the newly introduced dark scalar particle. The β parameter governs the mixing between the new dark scalar and the Standard Model Higgs. This is due to electroweak symmetry breaking. The Φ_{SM} field thus denotes the Standard Model Higgs doublet, while the Φ_D now denotes the new dark scalar singlet. These fields are described as

$$\Phi_{SM} = \frac{1}{\sqrt{2}}(h + v) \quad \Phi_D = \frac{1}{\sqrt{2}}(s + w), \tag{32}$$

where v is the vacuum expectation value (vev) belonging to the Standard Model Higgs, and w the vev of the dark scalar particle. The dark scalar field Φ_D has to produce a vev in order for the dark scalar to be able to interact with the dark photon. Without the vev, no interactions would be possible. Due to the β term, there is mixing between the Standard Model Higgs and the dark scalar. When inserting the fields, the relevant part of the potential becomes

$$V_0 \supset \frac{-\mu^2}{2} h^2 - \frac{3}{2} \lambda h^2 v^2 - \frac{\beta}{2\sqrt{2}} h^2 w - \frac{1}{2} m_s^2 s^2 - \frac{\beta}{\sqrt{2}} v h s. \tag{33}$$

The first three terms contain only the Higgs, the fourth term describes the mass of the dark scalar; $m_s^2 = \mu_s^2 + 3\lambda_D w^2$. The last term contains a mixing term between the two fields, thus the fields still have to be diagonalized, since this term cannot be interpreted as a mass term. This part of the potential can therefore be rewritten into a matrix notation. Where this matrix has to be diagonalized, in order to find the proper mass eigenstates of the system. The matrix is written in the basis of (h, s)

$$\mathcal{M}^2 = \begin{pmatrix} -2\mu^2 - \sqrt{2}\beta w & \beta v \\ \beta v & m_s^2 \end{pmatrix}. \tag{34}$$

The Higgs-Dark scalar mixing angle θ_ϕ that I found is thus the angle that allows for the diagonalization of the matrix shown above.

$$\tan\theta_\phi = \frac{m_s^2 - 2\mu^2 - \sqrt{2}\beta w \pm \Delta m^2}{\sqrt{2}\beta v} \tag{35}$$

Here, $\left(\Delta m^2\right)^2 = (-2\mu^2 - \sqrt{2}\beta w + m_s^2)^2 + 2\beta^2 v^2$ and $\lambda v^2 = -\mu^2 - \frac{\beta w}{\sqrt{2}}$.

So in mass-eigenstates, this results in

$$\begin{aligned} \tilde{h} &= h\cos\theta_\phi + s\sin\theta_\phi \\ \tilde{s} &= -h\sin\theta_\phi + s\cos\theta_\phi, \end{aligned} \tag{36}$$

where the fields with a tilde are the mass eigenstates. The Standard Model Higgs couplings need to remain the same, since they have been experimentally tested. Due to this, the $\cos\theta_\phi$ term needs to be close to 1, to ensure this. This means that the mixing angle θ_ϕ thus needs to be $\theta_\phi << 1$. For this model, this mixing angle is found to be $\theta_\phi \leq 0.008$. The derivation of this mixing angle can be found in appendix A. Through this scalar mixing between the Standard Model Higgs and the dark scalar, the dark scalar thus inherits all of the Higgs couplings. However, it does inherit them with a factor $\sin\theta_\phi$. Because this sine is thus very small, the inherited couplings will also be very small.

Thus, the dark scalar is now also able to couple to fermions through a Yukawa interaction, just like the Standard Model Higgs does. These new mass eigenstates result in Yukawa interactions of the form

$$\mathcal{L} \supset -\frac{y_f}{\sqrt{2}}\bar{f}_L f_R h + h.c. \Rightarrow \frac{-y_f}{\sqrt{2}}\left(\cos\theta_\phi \bar{f}_L f_R \tilde{h} + \sin\theta_\phi \bar{f}_L f_R \tilde{s}\right) + h.c. \tag{37}$$

From here on, all the fields will be mass eigenstates, unless told otherwise. This new Yukawa interaction describes now not only the interactions of the Standard Model Higgs h with fermions, but it also describes the interactions between the dark scalar s and fermions. The first term describes the Standard Model Higgs interactions, now with an extra $\cos\theta_\phi$ term. The second term describes the interaction between the dark scalar and fermions, with an $\sin\theta_\phi$ term. The $f\bar{f}$ denotes the fermion anti-fermion pair.

3.3 Branching ratios

After discussing all the relevant parts of the Lagrangian, it is possible to discuss the implications of these added Lagrangian terms. The new dark photon and

dark scalar particle allow for new interactions. In the following section, the decay branching ratios of the new particles will be discussed. Only the decay channels which are not suppressed will be discussed. Hence why only three processes are discussed here.

3.3.1 Decay of a dark scalar to a fermion pair

The fist decay of interest is the decay of a dark scalar going to a fermion anti-fermion pair. The process is shown in the following Feynman diagram.

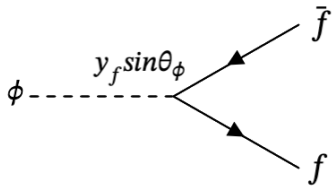

Figure 2: The Feynman diagram showing the decay of a dark scalar into a fermion anti-fermion pair. The strength of the interaction is dependent on the Yukawa coupling y_f and the sine of the Higgs-dark scalar mixing angle.

From equation 37, the relevant term for interactions between the dark scalar and Standard Model fermions can be found.

$$\mathcal{L} \supset -\frac{y_f}{\sqrt{2}} \sin\theta_\phi \bar{f} f s \tag{38}$$

The term scales with the Yukawa coupling y_f and the Higgs-dark scalar mixing angle, $\sin\theta_\phi$. The Yukawa coupling constant is dependent on the type of fermion anti-fermion pair that is produced, since $y_f = \sqrt{2}\frac{m_f}{v}$. The term $\sin\theta_\phi$ is the mixing angle between the Standard Model Higgs and the dark scalar mass eigenstates, as can be seen from 36. Because this interaction term scales with the sine of the mixing angle, it will be suppressed, since the Higgs-dark scalar mixing angle is very small. This means that the sine will also be very small.

With the use of this Lagrangian term, I was able to calculate the squared matrix element of the process of a dark photon decaying into a fermion anti-fermion pair. Using the squared matrix element, I found the following decay width, which is in accordance with [8].

$$\Gamma(s \to f\bar{f}) = \frac{1}{16\pi} m_s y_f^2 N_c \sin^2\theta_\phi \left(1 - \frac{4m_f^2}{m_s^2}\right)^{\frac{3}{2}} \tag{39}$$

Thus, the decay width scales with $\sin^2\theta_\phi$. Here, m_s denotes the dark scalar mass. N_c represents the number of colours, being three for quarks, and one for

leptons. As discussed above, the mixing angle of the Higgs-dark scalar will be very small. Since the decay width scales with the squared sine of this mixing angle, this decay width will be highly suppressed because of this.

3.3.2 Decay of a dark scalar to a dark photon pair

The next interaction is the decay of a dark scalar decaying into dark photon pair. This process can be seen in the following Feynman diagram.

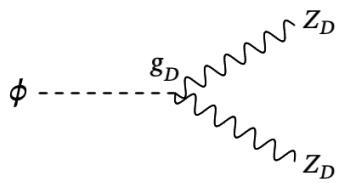

Figure 3: The Feynman diagram showing the decay of a dark scalar to two dark photons. The strength of this coupling is dependent on g_D, the gauge coupling of the dark sector.

The Lagrangian containing the interaction between the dark scalar and the dark photons is given by the gauge-kinetic term of the dark scalar, namely

$$\mathcal{L} \supset (D_\mu \Phi_D)^\dagger (D^\mu \Phi_D). \tag{40}$$

This is the same gauge-kinetic term as discussed in equation 23. After introducing the dark scalar fields to this equation, the gauge kinetic term becomes

$$\mathcal{L} \supset \frac{1}{8} g_D^2 Z_{D\mu} Z_D^\mu s^2 + \frac{1}{8} g_D^2 Z_{D\mu} Z_D^\mu w^2 + \frac{1}{4} g_D^2 Z_{D\mu} Z_D^\mu sw. \tag{41}$$

In this expression, the fields are not jet the diagonalized fields. The first term of this expression contains the interactions between two dark photons and two dark scalars. The second term contains the mass term of the dark photons. The third term contains the interaction between one dark scalar and two dark photons. All the fields are the fields before diagonalization.

From the second term, the mass term, it follows that

$$m_{Z_D} = \frac{1}{2} g_D w. \tag{42}$$

Now, after rewriting the fields in terms of mass eigenstates using equations 26 and 36, the two interaction terms thus become

$$\mathcal{L} \supset \frac{1}{8} g_D^2 \tilde{Z}_{D_\mu} \tilde{Z}_D^\mu \tilde{s}\tilde{s} cos^2\theta_D cos^2\theta_\phi + \frac{1}{4} g_D^2 \tilde{Z}_{D_\mu} \tilde{Z}_D^\mu \tilde{s} w cos^2\theta_D cos\theta_\phi. \tag{43}$$

Of these two terms, the second term describes a dark scalar decaying to two fermions, while the first term describes the interaction between two dark scalars and two dark photons. With the use of the found expression for the mass of the dark photon, this can be rewritten to (with the tildes again omitted)

$$\mathcal{L} \supset \frac{1}{2} m_{Z_D} g_D Z_{D\mu} Z_D^{\mu} s. \tag{44}$$

Here, all the terms with a squared cosine are omitted. This can be done since both θ_D and θ_ϕ are small, meaning that the squared cosine terms of these angles will become close to unity.

Next, I calculated the decay width belonging to the decay of a dark scalar to two dark photons. This decay width is given by

$$\Gamma(s \to Z_D Z_D) = \frac{1}{32\pi} g_D^2 \frac{m_{Z_D}^2}{m_s} \left(1 - \frac{4m_{Z_D}^2}{m_s^2}\right)^{\frac{1}{2}} \left(3 + \frac{m_s^4}{4m_{Z_D}^4} - \frac{m_s^2}{m_{Z_D}^2}\right). \tag{45}$$

Because both final state particles are Z_D, there is also an extra symmetry factor of $\frac{1}{2}$ involved in calculating this decay width. The found decay width agrees with [9].

Two of the above discussed decay widths contain interactions of a dark scalar decaying to two other particles, namely the fermion anti-fermion pair, and two dark photons. Now that the decay widths of these processes are known, they can be compared. As stated above, the process where the dark scalar decays into a fermion anti-fermion pair is highly suppressed by the squared sine of the Higgs-dark scalar mixing angle. However, the process where the dark scalar decays into two dark photons does not have this suppression, this process scales with the gauge coupling of the dark sector, g_D. Since this second process is not suppressed, this will be the dominant decay mode of the dark scalar, as long as g_D is sizeable and $m_s >> 2m_{Z_D}$. The branching ratio of dark scalars decaying to dark photons can be determined using the following equation.

$$BR(s \to Z_D Z_D) = \frac{\Gamma(s \to Z_D Z_D)}{\Gamma(s \to Z_D Z_D) + \Gamma(s \to f\bar{f})} \tag{46}$$

Because the decay width of dark scalars going to a fermion anti-fermion pair is thus negligible, the branching ratio will be close to 1. In the following, thus during the simulations, the branching ratio of a dark scalar decaying to two dark photons is assumed to be 1.

3.3.3 Decay of a dark photon to a fermion pair.

Now that the branching ratio of the dark scalars has been discussed, it is time to describe the decay of the dark photons. The decay process of these particles

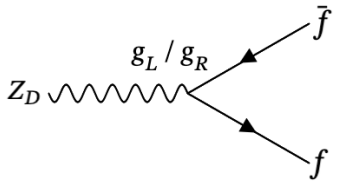

Figure 4: The Feynman diagram showing the decay of a dark photon into a fermion anti-fermion pair. The left- and right-handed couplings denote the strength of the interaction.

into two fermions can be seen in figure 4. This process is described by the Lagrangian terms

$$\mathcal{L} \supset g_L Z_{D\mu} \bar{f}_L \gamma^\mu f_L + g_R Z_{D\mu} \bar{f}_R \gamma^\mu f_R. \tag{47}$$

These new Lagrangian terms are a result of the kinetic mixing and electroweak symmetry breaking. Through this, the dark photon picks up the couplings of the Z boson, leading to the terms that are shown. This is because the B field picked up a dark photon component, as can be seen in equation 19. Because of this extra component, there will now also be Lagrangian terms describing an interaction between fermions and a dark photon. But not only the B field mixes, the mass eigenstates for the Z boson and the dark photon are mixed, as follows from equation 26. Due to this mass mixing, also the terms of the Z boson get an extra dark photon interaction with the fermions.

In the expression of the Lagrangian above, the diagonalized dark photon fields are represented by Z_D, and the fermion fields by f_L and f_R for left- and right-handed fermions, respectively. The γ^μ is a gamma matrix. g_L and g_R are the coupling strengths of the left- and right-handed fermions, respectively. The derivation of these coupling constants can be found in Appendix B.

$$g_L = \frac{g}{c_w}\left[-\cos\theta_d s_w \frac{Y_{w_L}}{2}\frac{\epsilon}{c_w} - \sin\theta_d\left(c_w^2 I_3 - s_w^2 \frac{Y_{w_L}}{2}\right)\right] \approx eQ\epsilon \tag{48}$$

$$g_R = \frac{g}{c_w}\left[-\cos\theta_d s_w \frac{Y_{w_R}}{2}\frac{\epsilon}{c_w} + \sin\theta_d s_w^2 \frac{Y_{w_R}}{2}\right] \approx eQ\epsilon \tag{49}$$

Here, g is the SU(2) gauge coupling, c_w and s_w are respectively the cosine and the sine of the Weinberg angle, θ_d the mixing angle between the dark photon and the Z boson. Y_{w_L} and Y_{w_R} the hypercharge of the fermion and I_3 the third component of the isospin. In the limit where the kinetic mixing parameter $\epsilon \ll 1$ and $m_{Z_D} \ll m_Z$, the coupling constants can be approximated to the last part of the equalities [10]. Here, e is the electric charge of the proton, Q the charge of the particle and ϵ the kinetic mixing parameter.

The decay width which I calculated belonging to the decay of a dark photon to two fermions results in the following expression, it also agrees with [11] and [5].

$$\begin{aligned}\Gamma(Z_D \to f\bar{f}) &= \frac{N_c}{24\pi m_{Z_D}} \left(1 - \frac{4m_f^2}{m_{Z_D}^2}\right)^{\frac{1}{2}} \left[m_{Z_D}^2(g_L^2 + g_R^2) - m_f^2(g_L^2 + g_R^2 - 6g_L g_R)\right] \\ &\approx \frac{1}{12\pi} N_C Q^2 e^2 \epsilon^2 m_{Z_D} \left(1 + \frac{2m_f^2}{m_{Z_D}^2}\right) \left(1 - \frac{4m_f^2}{m_{Z_D}^2}\right)^{\frac{1}{2}}\end{aligned} \tag{50}$$

Thus, the decay width of a dark photon decaying into a fermion anti-fermion pair scales with $\epsilon^2 m_{Z_D}$. The kinetic mixing parameter ϵ dictates how strong the dark sector couples to the SM particles, and is experimentally bounded, $\epsilon \sim 10^{-17} - 10^{-2}$ as stated above. Due to the ϵ having such small possible values, the coupling of the dark sector to SM will also be small. This means that the lifetime of the dark photons will be long, since the lifetime is inversely proportional to the decay width, and thus to ϵ^2. Thus, through the choice of kinetic mixing parameters ϵ, the lifetime of the dark photons can be set.

The dark photons can only decay into a fermion anti-fermion pair. For our benchmark scenario of interest, the relevant branching ratios are that of a dark photon decaying into electrons and into muons. The reason why these are the only fermions of interest here is because of the choice of mass of the dark photon. Since it is not possible for the mass of the fermion pair to exceed the mass of the dark photon. The mass of the dark photon here is chosen in such a way that the only resulting fermions are electrons and muons, so also no light mesons can be formed.

Thus these branching ratios will be

$$\begin{aligned}BR(Z_D \to e\bar{e}) &= \frac{\Gamma(Z_D \to e\bar{e})}{\Gamma(Z_D \to e\bar{e}) + \Gamma(Z_D \to \mu\bar{\mu})} \\ BR(Z_D \to \mu\bar{\mu}) &= \frac{\Gamma(Z_D \to \mu\bar{\mu})}{\Gamma(Z_D \to e\bar{e}) + \Gamma(Z_D \to \mu\bar{\mu})}.\end{aligned} \tag{51}$$

3.4 Dark scalar production

The dark scalars can be produced in flavour-changing transitions such as $b \to s\phi$ [12]. Here, the process that is used to describe the production rate is $B \to X_s\phi$. Where, X_s represents any final state with a strange quark. The model that is used to make predictions about the branching ratio of this process is the spectator model [13]. The spectator model neglects the mass of the light quark inside the meson, thus only looking at the decay of the bottom quark into the strange

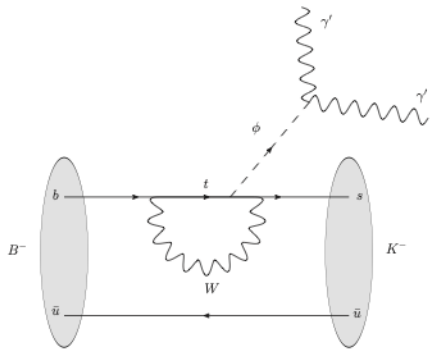

Figure 5: This figure shows the process through which the dark scalars are being produced [9]

.

quark, which is the quark-level process that is needed for the creation of dark scalar particles. However, since the mass of the other quark is neglected, and due to non-perturbative QCD effects, the spectator model overestimates the decay rates at low dark scalar mass. This is due to the neglect of the phase space suppression by the X_s mass [12]. The spectator model gives the best results when $m_\phi < m_B - m_K$, thus only for dark scalars with a low mass. However, above this mass, it still makes reasonable approximations.

Other models for determining the branching ratios are the Exclusive Model [14] and the Rescaled Model [15]. The Exclusive Model sums the branching ratios of the decays into specific meson final states. However, for low masses of the dark scalar, the Exclusive Model shows a deficit. The Rescaled Model uses a scaling factor on the branching ratios $BR_{B\to K\phi} + BR_{B\to K^*\phi}$. However, this approach differs a lot from the other two models.

In this research, the spectator model is used to determine the branching ratio of the dark scalar production. Here, the mass of our dark scalar is set far below the difference between the B meson and K meson masses, thus $m_S << m_B - m_K$. The spectator model predicts the following decay width [13]

$$\Gamma_{B\to X_s\phi} = |g_{\phi sb}|^2 \frac{\left(m_B^2 - m_\phi^2\right)}{32\pi m_B^3}. \tag{52}$$

With m_B and m_ϕ the masses of the B meson and the dark scalar, respectively. The prefactor $g_{\phi sb}$ is given by [13]

$$g_{\phi sb} = \frac{\sin\theta_\phi m_b}{v} \frac{3\sqrt{2} G_F m_t^2 V_{ts}^* V_{tb}}{16\pi^2}, \tag{53}$$

as a result of integrating out the W boson and top loop, as seen in figure 5. Here, V_{ts} and V_{tb} are the CKM matrix elements and G_F the Fermi constant. Thus, the decay width of the B decaying to a dark scalar scales with the squared sine of the Higgs-dark scalar mixing angle. From this, the branching ratio can be formulated

$$BR(B \to X_s\phi) = \frac{\Gamma_{B\to X_s\phi}}{\Gamma_{\mathrm{B}} + \Gamma_{B\to X_s\phi}}. \tag{54}$$

Where Γ_B is the decay width of all the Standard Model decays of the B meson.

The relevant aspects of the dark sector model have been discussed. Production of the dark scalars from the B mesons has been described and the decay width is described. Next, the dark scalar has been described. The dark scalar will promptly decay into a dark photon pair, with a branching ratio of 1. Finally, the dark photons have been described. Due to their inverse relation to ϵ, they are long-lived particles, with a small mass. They can decay into a fermion anti-fermion pair, as described by the given branching ratios.

3.5 Full decay chain

Now that all the aspects of the dark sector model have been discussed, it is possible to write down the full decay chain.

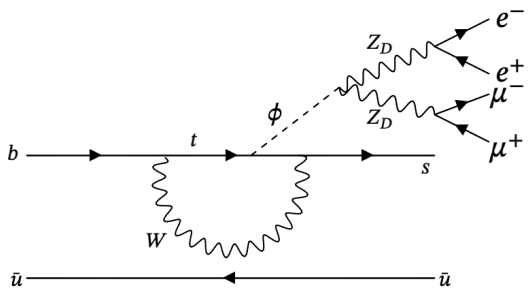

Figure 6: This Feynman diagram shows the full decay chain starting from a B meson. The dark scalar is produced through a W top loop. The dark scalar decays into a dark photon pair. The dark photons decay into either an electorn or a muon pair.

- **Dark scalar:** the dark scalars are a decay product of the B meson. The decay width of the process $B \to X_s\phi$ scales with a factor sine squared of the Higgs-dark scalar mixing angle and will thus be quite small, $\theta_\phi \leq 0.008$, see appendix A. The dark scalar itself is an addition to the Standard Model that was added though a Higgs portal. The dark scalar mixes with

the Standard Model Higgs, through which it inherits all of the Standard Model Higgs couplings, all be it with a factor $\sin\theta_\phi$ added. The dark scalar also acquires a vev w. The decay of the dark scalar leads to the production of two dark photons, with a branching ratio of 1.

- **Dark photon:** the dark photon is thus a result of the decay of a dark scalar. The dark photon is also an extension of the Standard Model. It is introduced through kinetic mixing with the hypercharge field, where the mixing is determined by the kinetic mixing parameter ϵ. After a shift of the fields and diagonalizing the appropriate terms, there is mixing found between the dark photon and the Standard Model photon. Through this, the dark photon can inherit the couplings. The dark photon can thus decay into a fermion anti-fermion pair. However, because of the choice of mass, the only possible fermions that it can decay into are electrons and muons. The lifetime of the dark photon is inversely proportional to the decay width, thus inversely proportional to ϵ^2. Through this, the kinetic mixing parameter determines the lifetime of the dark photons.

In the beginning of this chapter, the needs of the benchmark model were discussed. As said, the particles which are going to travel to the FASER and ATLAS detectors need to be light. The dark photon mass is already bounded from above by the masses of the B and K mesons, $m_{Z_D} < (m_B - m_K)/2$. This already sets the dark photon mass up to be light. Next, the lifetime of the dark photons had to be long, since long-lived particles were needed to be able to reach the FASER detector. As described above, the lifetime of the dark photons is inversely proportional to the square of the kinetic mixing parameter ϵ. The value of the kinetic mixing parameter is experimentally found to be lower than 10^{-2}, already leading to long lifetimes of the dark photons. Selecting smaller values for ϵ will make the lifetime of the dark photons longer. At last, two particles needed to be created, which is also the case here, since the dark scalar decays into two dark photons.

4 Detectors

In order to facilitate the detection of particles that are the decay products of the dark photons, here electrons and muons, the use of detectors is appropriate essential. The two relevant detectors in this research are the ATLAS and the FASER detectors. Both detectors are located at the LHC. The ATLAS detector is a large, multi-purpose detector, that is located as a barrel around the point where the particle beams cross, the interaction point (IP). Consequently, particles that travel in the transverse direction will be detected by the ATLAS detector.
The FASER detector, in contrast to the ATLAS detector, is not a barrel detector surrounding the interaction point. Rather, it is located 480 meters downstream from the interaction point, along the beam collision axis. The primary objective of the FASER detector is to detect particles, or decay products thereof, that are boosted in the far-forward direction. In addition, these particles also need to be long-lived, light and weakly interacting to be able to traverse the entire distance of 480 meters without undergoing any interactions. It is only under these conditions that it is possible to decay within the FASER detector.

4.1 ATLAS

The ATLAS detector is a large multi-purpose detector located at one of the interaction points (IP) of the Large Hadron Collider (LHC). The operation of the ATLAS detector started in 2009, with various upgrades during shutdown periods [16].

- **Run 1 2009-2013:** Centre-of-mass energy of $\sqrt{s} = 7$ TeV, with an integrated luminosity of 5 fb^{-1}. During this run, the centre-of-mass energy was also increased to $\sqrt{s} = 8$ TeV, resulting in an integrated luminosity of 21 fb^{-1}. All the mentioned integrated luminosities are for proton-proton collisions.

- **Run 2 2015-2018:** The centre-of-mass energy during this run was achieved to be $\sqrt{s} = 13$ TeV, leading to an integrated luminosity of 147 fb^{-1}.

- **Run 3 2022-2025:** An integrated luminosity of 160 fb^{-1} has been achieved per September 2024 for proton-proton collisions [17]. The centre-of-mass energy that is achieved for this run is $\sqrt{s} = 13.6$ TeV.

- **High Luminosity Large Hadron Collider (HL-LHC) 2029 and later:** The expected integrated luminosity of the HL-LHC is approximated to be 250 fb^{-1}, per year of operation. The goal is to achieve 3000 fb^{-1} in around 12 years after the upgrade. The centre-of-mass energy that is hoping to be achieved is 14 TeV. [18]

The ATLAS detector can be divided into various segments. For this research, the most interesting part of the ATLAS detector is the segment that is located right around the interaction point and has the biggest range of detecting

particles which are more forward-going. Currently, the closest detector part to the interaction point is the Inner Detector. However, this Inner Detector is only sensitive to particles which have a pseudorapidity smaller than 2.5.

During the downtime of the LHC between run 3 and run 4 with the HL-LHC, the ATLAS detector will also be upgraded. One of the upgraded parts is this Inner Detector, which will be replaced by the Inner Tracker (ITk) [19]. The ITk will consist of an inner pixel detector, as well as an outer barrel detector and an outer end-cap. The ITk will increase the pseudorapidity coverage of the detector, going to an accepted pseudorapidity of $|\eta| < 4$ [19], as opposed to the $|\eta| < 2.5$ of the current Inner Detector. Hence why for this research the Inner Tracker will be discussed.

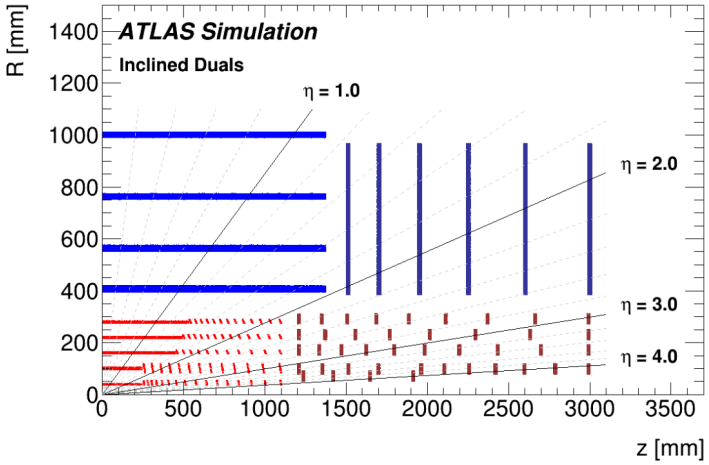

Figure 7: This figure shows the schematics of the ITk. The part in red represents the inner pixel detector, the light red part is the barrel part, the dark red section represents the end-cap rings of the pixel detector. The blue part is the strip detector, where the horizontal lines again represent the barrel part, and the verticals the end-cap rings [19].

The Inner Tracker consists of an outer barrel, outer endcap and an inner barrel and endcaps. The inner most detector part of the detector consists of silicon pixels. The outer regions consist of silicon strips [19]. The detector is 1 meter high and 3 meters long, as can be seen from figure 7.

- **Strip Detector:** The strip detector consists of four barrel layers and six endcap disks. These are shown in blue in figure 7. In light blue the barrel layers are shown, in dark blue the endcap disks can be seen. The Strip Detector covers a pseudorapidity range of $|\eta| < 2.7$.
- **Pixel Detector:** The pixel detector is also shown in figure 7, in red. The

light red parts are the barrel layers, and the dark red part indicates the endcap rings of the Pixel Detector. The Pixel Detector gives the Inner Tracker a total pseudorapidity coverage of $|\eta| < 4$.

From figure 7 it can also be seen that the height of the detector is 1 meter, and the maximum distance from the interaction point is 3 meters. Thus, the new Inner Detector will be sensitive to a bigger range of pseudorapidity values of the particles. This is very useful for this research. The bigger the pseudorapidity range of the Inner Tracker is, the smaller the opening angle of the two dark photons may be. Because the particles will be produced in the forward direction, it will be hard to produce them with very large opening angles. Hence why a bigger pseudorapidity range of the detector is of the highest importance.

4.2 FASER

Just like the ATLAS detector, the FASER detector [20] is suited to search for particles that are created at the interaction point at the LHC. However, unlike the ATLAS detector, the FASER detector is not located as a barrel around the interaction point. Instead, it is located along the beam collision axis, 480 meters downstream from the interaction point. The FASER detector searches for light, weakly-interacting particles that are a result of the proton-proton collisions at the interaction point. Some of these light and weakly-interacting particles are long-lived particles, allowing them to easily traverse the 480 meters from the interaction point to the FASER detector.

Thus, the FASER detector can be used to detect the decay products of these long-lived, light, and weakly interacting particles. These particles are mainly produced in the forwards direction, along the beam axis. Since the ATLAS detector is located around the beam axis as a barrel, it cannot detect particles that are boosted in the very forwards direction. As stated above when discussing the ATLAS detector, the inner detector only can detect particles with a pseudorapidity of $|\eta| < 2.5$, and the future inner tracker is only sensitive to $|\eta| < 4$ particles. This means that these particles that travel in the forward direction, cannot be detected by the ATLAS detector.

However, the FASER detector is located specifically along the beam collision axis, allowing for detection of the decay products of these particles. The FASER detector has a decay volume of length L = 1.5 meter, and a radius of R = 10 cm. Due to the geometry of this decay volume and the location of FASER, only particles with a pseudorapidity of $\eta > 9.2$ can decay inside this decay volume [20]. Thus, only particles that are extremely boosted towards the beam collision axis have a chance to decay in FASER.

The FASER detector consists of various parts, described from where the particles first enter the detector:

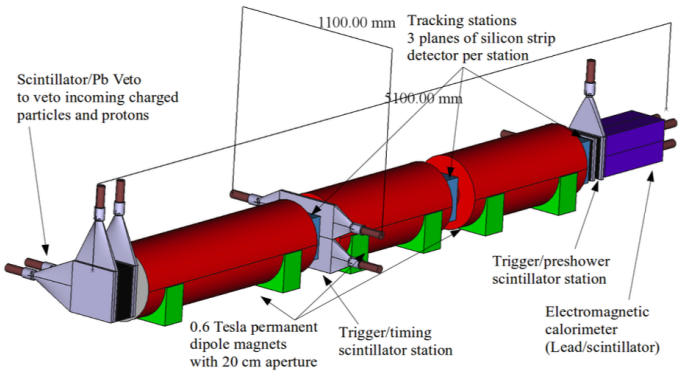

Figure 8: This figure shows a schematic representation of the FASER detector. The particles coming from the interaction point enter the detector from the left. The gray parts are the scintillators, the red parts the magnets, of which the first one is the decay volume. The blue parts are the tracking station, and the last part in purple represents the calorimeter [20].

- Two scintillators, which veto the charged particles that are coming through the wall from the interaction point. In-between these two scintillators is a lead plate, which prevents photons to enter the detector by converting them to electromagnetic showers, which the scintillators will take care of.
- The decay volume of the detector. As stated above, the decay volume has a length of L = 1.5 meter, and a radius R = 10 cm. Since the detector is also located 480 downstream from the interaction point, this results in a sensitivity to particles with a pseudorapidity of $\eta > 9.2$. The decay volume consist of a 0.6 T dipole magnet. When the decay products are a pair of charged particles, the magnet will separate the decay products, to be able to detect both the decay products separately.
- After the decay volume, there are three tracking stations, separated by two additional 0.6 T magnets. Just like the magnet of the decay volume, these magnets also separate the decay products, to make clearer tracks of both particles separately.
- The last part of the FASER detector is an electromagnetic calorimeter. This measures the total electromagnetic energy of the electromechanically charged decay product.

As stated above, the detector is located along the beam collision axis. However, in order for the detector to be placed along the axis, the beam already needs to be curved away. Because of this, the FASER detector is built 480 meters downstream from the interaction point. This also means that the particles that want to reach FASER have to traverse 10 meters of concrete and 90 meters of rock. However, since the FASER detector is located within a maintenance

shaft of the LHC, there is only empty space 5 meters before the detector, as can be seen in figure 9. Because of this, it is also possible for dark photons to decay within this volume before the detector and still have their decay products be detected within the FASER detector.

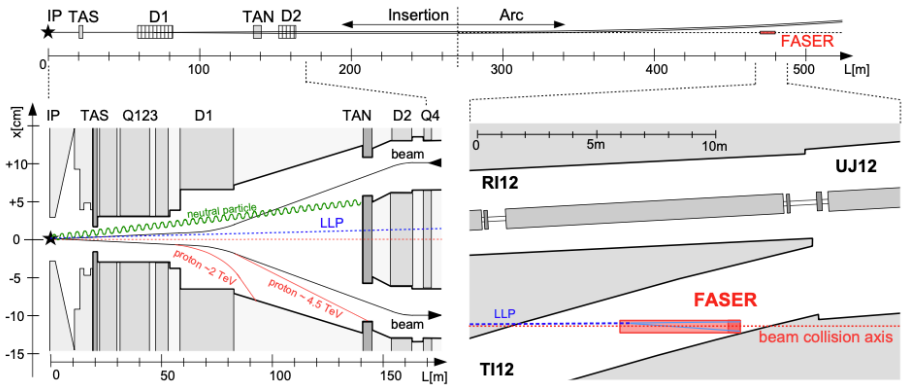

Figure 9: This figure schematically shows the location of the FASER detector relative to the beam axis. The top part of the figure shows the interaction point (IP) and the location of the detectors surrounding it along the beam axis. At 480 meters, the FASER detector is shown. On the lower left, a zoomed in view on the interaction point is shown, together with detectors surrounding it. The coloured lines show how different types of particles that are produced in the far-forward direction traverse through this section, with the long-lived particle (LLP) following the beam collision axis, without being absorbed. The bottom right side of the figure is zoomed in on the FASER detector. Here, it can clearly be seen that the FASER detector is located along the beam collision axis, which is shown by the red dotted line.

So in total, particles need to have a pseudorapidity higher than 9.2 to be able to decay within the FASER detector. The decay volume of the FASER detector itself is 1.5 meters long, starting 480 meters from the ATLAS interaction point. Due to the maintenance shaft where the FASER detector is located, it is also possible to detect particles which decay 5 meters before the FASER detector, thus 475 meters away from the interaction point.

So in order for a dark photon pair to be able to decay within both the FASER and the ATLAS detector, the opening angle of the two particles needs to be substantial. Since the maximum sensitivity of the Inner Tracker is $|\eta| < 4$, while the FASER detector can only begin to detect particles with $\eta > 9.2$. Thus there is a substantial pseudorapidity gap between the two detectors. If a dark photon were to have a pseudorapidity that would lead it to travel to this gap, neither detector is able to detect it.

5 Event Simulations

5.1 PYTHIA

Now that the dark photon model and the detectors have been discussed, the phenomenology of the newly added particles can be discussed. The primary objective is to determine whether it is possible to detect two dark photon siblings in both the ATLAS and the FASER detectors, and to study the behaviour of the dark photons. Simulations of collision events are a useful tool to see how the dark photons might behave in collisions, and to determine where they could end up. For this research, the generation of the collision events is performed by the software tool PYTHIA [21]. PYTHIA is an event generator for collisions of high-energetic particles, such as are happening in the LHC.

PYTHIA v8.3 [22] is a code library, used to generate events of collisions between high-energetic particles, and is thus a so-called event generator. An event is the result of a collision between two particles, or the decay of one. Because the particles are highly energetic particles, and due to the statistical nature of QFT, the number, and the properties, of outgoing particles vary per event. A set of calculated probability distributions is used to determine the predicted event rates. An event generator is thus described as:

> 'A numerical algorithm that can produce (or "generate") random sequences of such simulated events, one after the other, is called an "event generator". The simulations can be based on known or hypothetical laws of nature. This allows for the exploration and comparison of competing paradigms, and studies of the sensitivity of proposed physical observables to the differences' (Bierlich et al., 2022, p. 8).

Thus, an event, especially for high-energetic collisions, is roughly a list containing the sub-atomic particles which are produced, along with a measure of the probability for that event to occur. In PYTHIA, this list also contains the four-momenta, production point and other properties of each particle. This list is what is called an "event record" in PYTHIA. However, the results of an event generator like PYTHIA are very dependent on the input parameters, up to an order of $\mathcal{O}(100)$ [21]. A collection of parameter values is called a tune.

5.2 Input choices

As stated above, the input parameter choice is very important when making simulations. The choices of input parameters are shown in table 1.

The mass of the dark photons is chosen to be $m_{Z_D} = 0.35$ GeV. Choosing this value guarantees that the decay products of the dark photons can only be electrons and muons [6]. Pions, the lightest mesons, are forbidden, due to their larger masses. The dark scalar mass is set to be $m_\phi = 1$ GeV. It of course

Table 1: This table shows the values of the input parameters used in the simulations.

Parameter choices	
Dark photon mass m_{Z_D}	0.35 GeV
Dark scalar mass m_ϕ	1 GeV
Kinetic mixing parameter ϵ	$3 * 10^{-7}$
Higgs-dark scalar mixing angle θ_ϕ	0.008
dark sector gauge coupling g_d	0.35
Centre of mass energy	14 TeV

has to be possible for one dark scalar to decay into two dark photons requiring $m_\phi > 2m_{Z_D}$. Also, the mass of the dark scalar is limited due to B meson decay where it is created. The mass of the dark scalar cannot exceed $m_B - m_K$.

The kinetic mixing parameter ϵ is set to $\epsilon = 3 * 10^{-7}$. This parameter is especially fine-tuned in these simulations, in order for the dark photons to be able to reach FASER. The lifetime of the dark photon is inversely proportional to $m_{Z_D}\epsilon^2$. Since m_{Z_D} is fixed, as stated above, the lifetime of the dark photon can be changed by changing the value of ϵ, as can be seen from figure 10. Here, the location of the dark photon decays can be seen along the beam collision axis for different values of the kinetic mixing parameter. The blue value, $\epsilon = 10^{-6}$, leads to the bulk of the dark photons decaying before the FASER detector. However, when going one order of magnitude lower, nearly all dark photons overshoot the FASER detector, as can be seen from the green line. When the kinetic mixing parameter is set to $\epsilon = 3 * 10^{-7}$, many dark photons will decay around the FASER detector. Using this value, and the decay width obtained in equation 50, the lifetime of the dark photons can be obtained, namely $\tau_{Z_D} = 4.422 * 10^{-9}$ seconds, or 1325.792 mm/c as used by PYTHIA.

The Higgs-dark scalar mixing angle θ_ϕ is constrained to be small, namely $\theta_\phi \leq 0.008$ A. This mixing angle can also be found in the decay width of $\Gamma(s \to Z_D Z_D)$. Just like with θ_D, the cosine terms of this angle go to one, because of the small value for θ_ϕ. The other place where θ_ϕ appears is in the decay width of $\Gamma(B \to X_s\phi)$. Here, θ_ϕ determines how big the branching ratios $BR(B^0 \to X_s\phi)$ and $BR(B^\pm \to X_s\phi)$ are. Thus, a small value for θ_ϕ will only limit the dark scalar production rate. Due to this, the term $\sin^2(\theta_\phi)$ in the branching ratio for the production of dark scalars is set to 1, and later the event rates are rescaled. This is to ensure that more dark scalars will be produced in the simulations.

The dark sector gauge coupling g_D only shows up in the expression of the decay width $\Gamma(s \to Z_D Z_D)$. The value of g_D is chosen such that the coupling $\alpha_D = 0.01$, since $\alpha_D = \frac{g_D^2}{4\pi}$. Through this parameter choice, the dark scalar

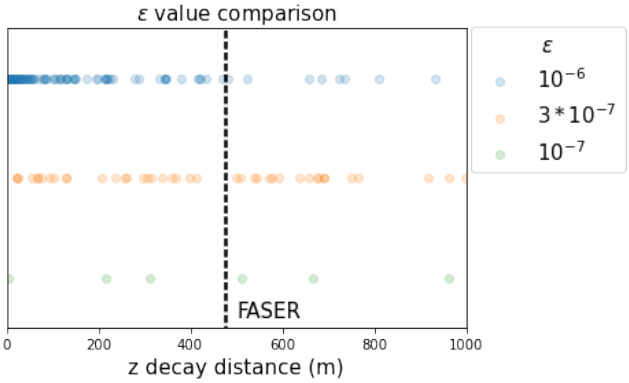

Figure 10: This figure shows the decay distance along the z axis, the beam collision axis, of dark photons with a pseudorapidity $\eta > 9.2$. The three different lines indicate different values for the kinetic mixing parameter ϵ. The black dashed line indicates the location of the FASER detector. 10^6 events were used for this plot.

lifetime can be calculated to be $1.6 * 10^{-10}$ mm/c. Thus, the dark scalar has a prompt decay, since the lifetime is extremely small. As explained above, the branching ratio of a dark scalar into fermions is highly suppressed. Thus, only the process of a dark scalar to dark photon pair is taken into account in the simulations.

The initial particles are both set to be protons, in order to properly simulate LHC data. The centre of mass energy of the initial interaction is set to 14 TeV. This value is chosen to be in accordance with the projected centre of mass energy of run 4 of the LHC, since the detector which is used for the simulations, the Inner Tracker, is also in use starting from run 4.

Table 2: This table shows the parameters that follow from the input parameters found in table 1 and the appropriate equations stated in chapter 3

Resulting values	
dark scalar lifetime	$1.6 * 10^{-10}$ mm/c
dark photon lifetime	1325.79 mm/c
$B^0 \to X_s\phi$ branching	$5.683 * 10^{-5}$
$B^{\pm} \to X_s\phi$ branching	$5.730 * 10^{-5}$
$\phi \to Z_D Z_D$ branching	rescaled to 1
Dark photon branching electrons	0.51
Dark photon branching muons	0.49

The lifetimes and branching ratios calculated from these chosen input parameters can be seen in table 2. Using these values, the simulations were made. In order to simulate LHC collision events, the centre of mass energy is set to be 14 TeV, and both incoming beams are protons. Also, hard b-bbar processes are turned on via `HardQCD:hardbbbar = on`, to make sure more B mesons are created, leading to more dark scalars. This setting is a tune, as mentioned before. Regarding the dark photons, the flag `isResonance = false` also has to be added, since it is a long-lived particle. This is to ensure the long-lived behaviour of the dark photons. Next to this, the command `rescaleBR = 1` has to be used, to ensure the total branching ratios to be rescaled to 1. For the dark scalar, the width of the Breit-Wigner distribution has to be added, which is the decay width of the dark scalar going to dark photons.

The files used for the simulations, as well as the most important data analysis methods can be found on git via: `https://gitlab.science.ru.nl/lbroekhoven/master-stage`.

5.3 Lifetime efficiency

Processing the data that is generated in the steps described above is a very time and GPU consuming process, due to the strong geometric constraints from both detectors, and the randomness of the decay distance per event. The chances of finding a dark photon which decays in the FASER detector are already quite slim. This is because the particle itself needs to be extremely boosted in the far-forwards direction, since the particle needs to have $\eta > 9.2$ in order to be able to decay within FASER. This already leads to a big reduction in the amount of usable data. Next to this, the decay volume of FASER is also quite small, the decay volume is 1.5 meters, and the empty shaft before that is 5 meters long. This means that the particles need to decay within 6.5 meters, in order to be able to be detected. Due to these two factors, the amount of dark photons found in the simulations which decay within FASER is very low.

The first way of improving the number of dark photons which end up in FASER is by fine-tuning the kinetic mixing parameter ϵ. As explained above, this parameter dictates how strong the dark sector mixes with the Standard Model particles. Due to this, the lifetime of the dark photon is inversely proportional to ϵ^2. This can intuitively be seen: when the dark sector and the Standard Model mix more easily, a higher ϵ, it is easier for the dark photon to decay into Standard Model fermions, thus leading to a shorter lifetime of the dark photon. Thus, by changing the value of ϵ, an optimal dark photon lifetime can be obtained for the decay within the FASER detector. The optimal result for this value of ϵ can be found in table 1.

Next to selecting an optimal value for ϵ, a pT-cut is made on the simulated data. The aim of the pT-cut is to increase the number of dark photons with a higher pseudorapidity. A pT-cut has no consequence to the sensitivity of

the model, however, it can improve the amount of useful data. By setting an upper bound for the pT of the dark photons, the particles with high pseudorapidity will still be simulated, however, there will be fewer particles with lower pseudorapidity. Due to this, a higher portion of the particles generated in the simulation will have a higher pseudorapidity. This will increase the chances of finding dark photons that can decay within FASER in a fixed event sample. This can also be seen in figure 11. The most optimal scenario would have been to apply a pseudorapidity cut, however, this is not an option in PYTHIA.

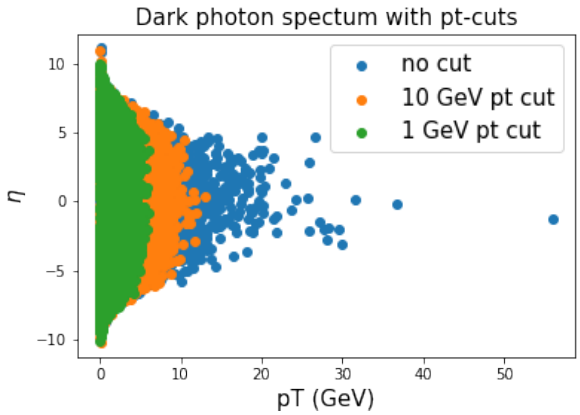

Figure 11: This figure shows the dark photon pT spectrum for three different pT-cuts. The blue region shows the pT of the dark photons without a pT-cut. Here, there are a lot of dark photons with low pseudorapidity. The orange area shows the dark photons with a 10 GeV pT-cut. Here, the peak around the lower η values is no longer present, as it was for the dark photons without a pT-cut. Lastly, the green area shows the dark photons with a 1 GeV maximum for the pT. Here, there are even less dark photons with lower η values simulated. For each of the shown cuts, 1000000 events were used.

After I tried to improve the number of dark photons found in FASER using the methods described above, another approach was needed, since the efficiency of the simulations was still unsatisfactory. This new approach will be called the 'probabilistic approach'. For this probabilistic approach, instead of analysing the final output from PYTHIA, only the information about the particles' energy and pseudorapidity is used. In the previous two methods, PYTHIA decided where the particles would decay, based on, among others, their lifetime and energy. Through this method, information about the probability to decay within FASER is lost, since the particle either does or does not end up in FASER. In order to regain this information, only the energy of the particles and their pseudorapidity will be extracted from PYTHIA. Using the pseudorapidity, it is possible to determine whether or not a particle geometrically could decay within FASER or ATLAS. Using the energy of the particle, the probability for decay can be calculated using the following two equations.

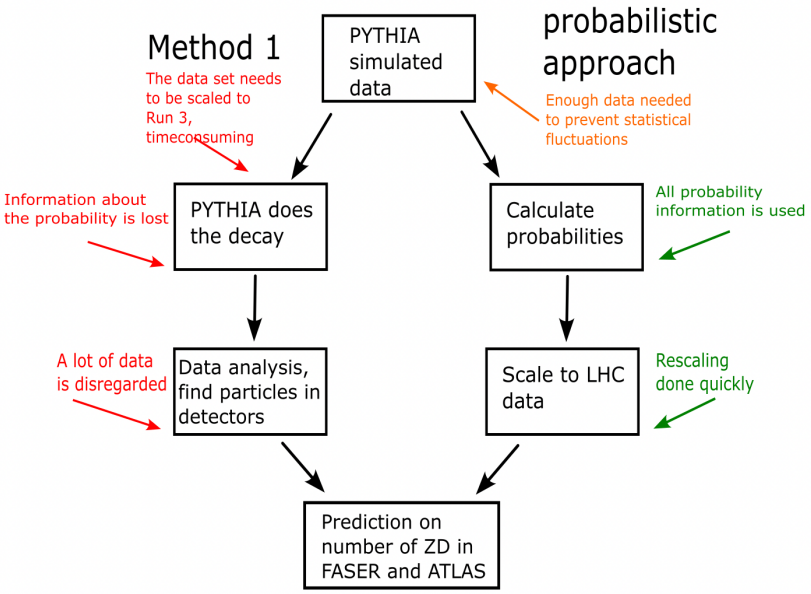

Figure 12: This figure shows a schematic overview of the the two described methods for the simulations and data analysis. The left side of the figure shows the first described method. On the right side, the probabilistic approach is shown. The annotations in red show the downsides of a certain step. The annotations in greed show positive properties of the methods. The orange annotation indicates a neutral step.

$$\mathcal{P}_{detector}(p) = exp\left(\frac{-r_{min}}{d(p)}\right) - exp\left(\frac{-r_{max}}{d(p)}\right) \quad \text{where} \quad d = \frac{p\tau}{m} \tag{55}$$

Here, r_{min} represents the minimum radial distance and r_{max} the maximal radial distance of the detector, p the momentum of the particle and τ the lifetime of the particle. The equation that I found here also coincided with [8]. For FASER, r_{min} is set to 475 meter and $r_{max} = 480$ meter. For ATLAS, r_{min} and r_{max} are dependent on the pseudorapidity of the dark photons, since the ATLAS ITk is a cylinder and thus not spherically symmetric. For the distances of the FASER detector, this is not a problem. Because the detector is only reachable for particles with a pseudorapidity > 9.2, the particles will all travel straight through the detector and we can neglect the η dependence of the decay volume. The parameter p represents the momentum of the particle, τ the lifetime, and m its mass.

Using both the information about the particles' direction, or pseudorapidity, and the probability of their decay, it is possible to determine the probability for

the dark photons to end up in FASER and ATLAS. Using this information, it is also possible to calculate the probability for one of the siblings to decay within the ATLAS detector, and for the other sibling to decay within FASER. This total probability can be obtained by multiplying both probabilities with each other.

$$\mathcal{P}_{\text{both siblings in detectors}} = \mathcal{P}_{\text{ATLAS}}(\text{sibling 1}) * \mathcal{P}_{\text{FASER}}(\text{sibling 2}) \tag{56}$$

Here, $\mathcal{P}_{\text{ATLAS}}$ and $\mathcal{P}_{\text{FASER}}$ are the probabilities of the dark photon decaying with FASER or ATLAS, as calculated by equation 55. Since the pseudorapidity ranges for the detectors do not overlap, the probability for a particle to decay in the other detector is always 0. Or, as described in the equation above, the probability to find sibling 1 in FASER or sibling 2 in ATLAS is 0. Hence, why these probabilities are omitted in the given equation above. Through this probabilistic approach, it is possible to scale up the number of particles from the PYTHIA simulations to LHC data. PYTHIA can also return the cross section σ of processes. Using this information, the number of B mesons that are produced in run 4 can be determined, using the integrated luminosity $\mathcal{L}_{int}$ of LHC run 4. The number of dark scalars produced during this run can then be determined via the branching ratio $BR(B \to X_s\phi)$. Now, a scaling factor can be determined between the number of dark scalars found in the simulated data and LHC run 4.

$$N_B = \sigma_B * \mathcal{L}_{int} \qquad\qquad N_\phi = N_B * BR(B \to X_s\phi)$$

This probabilistic approach is considerably more efficient than the method discussed prior, even with the two discussed improvements, showing an improvement of $\mathcal{O}(\infty^{\ni})$. With the first method, a considerable amount of data was disregarded, since only very few dark photons decayed exactly within FASER. With the probabilistic approach, all of the simulated dark photon data with proper pseudorapidity is used to determine the probabilities of these particles to end up in FASER or ATLAS. Later, these probabilities will be scaled up to LHC run 4 data.

6 Results

6.1 Method 1

Using the input setting from section 5.2, simulations can be made. PYTHIA is able to return a lot of information about the particles and the simulated events. First, the results of the output from PYTHIA are discussed, thus what is in section 5.3 called 'Method 1'.

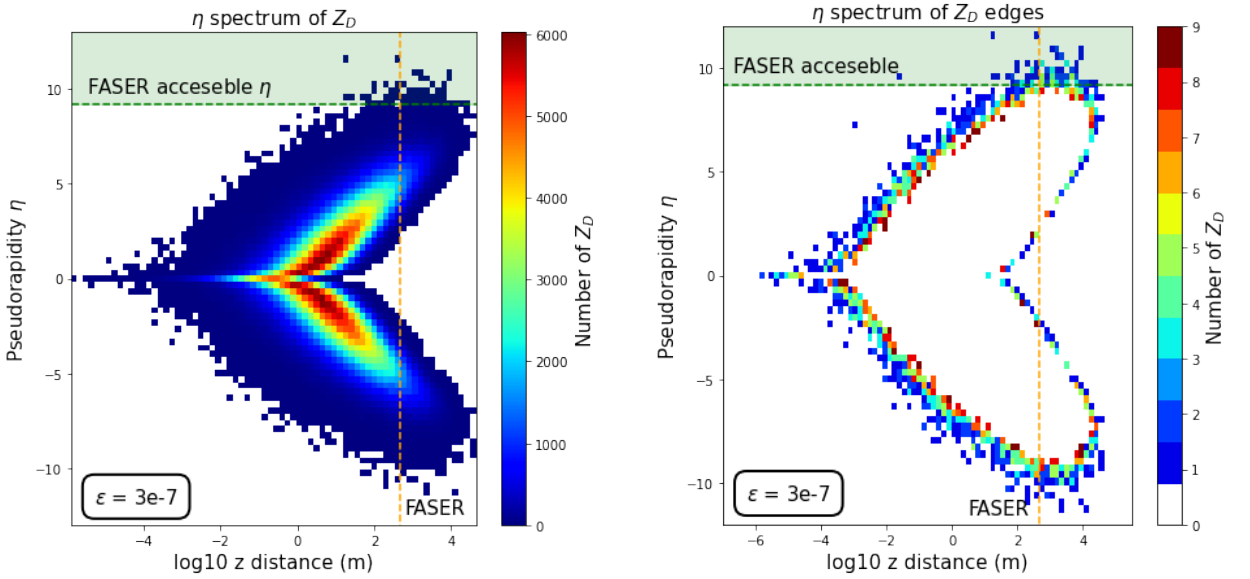

(a) Complete data set

(b) Only the bins with a number of $Z_D < 10$ are shown.

Figure 13: This figure shows the relation between the distance at which the dark photons decay in the direction along the beam axis, here called 'z distance', and the pseudorapidity η of the dark photons. The dashed orange line shows the distance to the FASER detector. The green dashed line indicates the minimal pseudorapidity needed for the particles to be able to decay within the FASER detector, $\eta > 9.2$. The green region shows where the pseudorapidity is sufficient in order for the particles to reach FASER. The simulations that were done for the creation of these plots were made with ϵ = 3e-7, and 1000000 events were generated for these figures.

In figure 13 the relation between the decay distance along the beam axis and the pseudorapidity of dark photons can be seen. Here, the green area indicates the region where the pseudorapidity is larger than 9.2, which is the minimum that is needed to go in the direction of the FASER detector. Since the FASER detector is only located on one side of the interaction points, only the top lobe of the figure is eligible to end up in FASER. As can be seen in the plot, there

are a few particles which can make it to this region. Thus, these particles go in the direction of the FASER detector. However, the FASER detector does not cover the whole of the green section. Since it is only located 475 meters away from the interaction point. This is indicated by the orange line. Thus, only particles that decay on the orange line within the green sector decay within FASER.

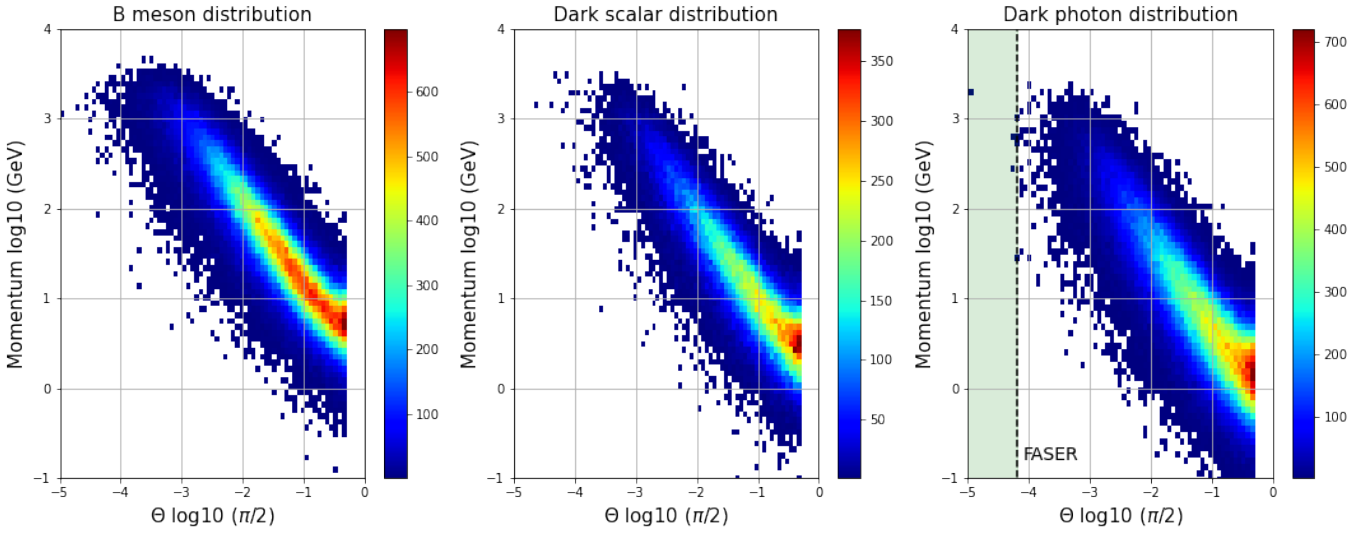

Figure 14: These figures show the relation between the angle with respect to the beam collision axis and the momentum of the particles. Both scales are logarithmic. The plot on the left shows the distribution of the B mesons. The plot in the middle shows the dark scalar distribution. Finally, the plot on the left shows the distribution of the dark photon. In this plot, the green shaded area represents where the angle of the particles is small enough in order to reach the FASER detector; thus where the angle corresponds to a pseudorapidity bigger than 9.2. For the creation of these plots, the information from 1000000 events was used again.

Figure 14 shows all particles in the decay process to get to the dark photons. The B mesons are already dominantly produced in the forward direction, as can be seen in the left-most plot. This sets up the decay products, here the dark scalars, to also travel in the forward direction. The dark photons that are a result of these forward-going dark scalars, will also dominantly travel in the forward direction. This can be seen in the right-most plot. The green area of the plot indicates where the dark scalars have a high enough pseudorapidity to end up in FASER. Here, a couple of dark photons with high momentum can be found that meet this criterion. However, the number of particles within this region is quite small.

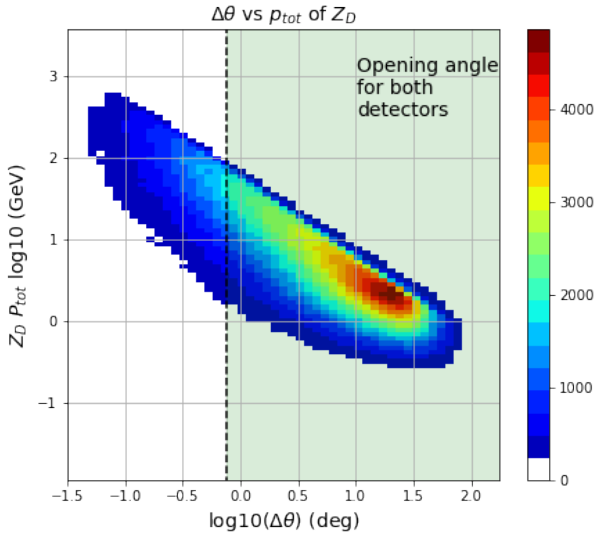

(a) Complete figure showing the opening angle of all the dark photon pairs. For this figure, 1000000 events were generated.

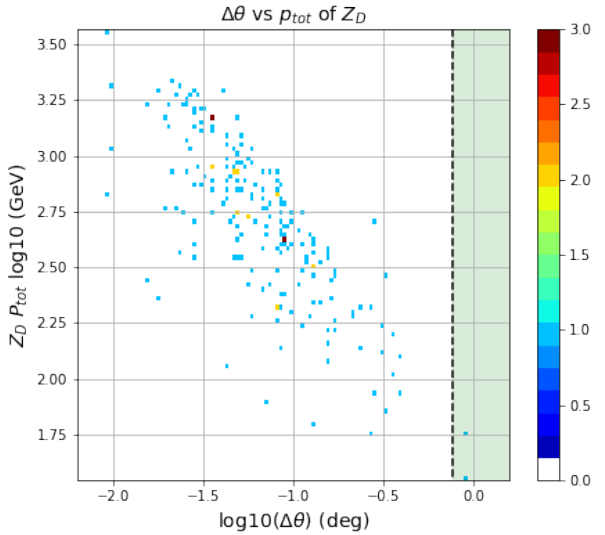

(b) Only sibling pairs of which one of the dark photons has $\eta > 9.2$ are shown. The green area again indicates the opening angle for both detectors.

Figure 15: Here, the opening angle $\Delta\theta$ of the dark photons is shown compared to the total momentum of the pair. In light green the region where the dark photon pair has a big enough opening angle to decay both in their respective detector is shown. The figure of the left shows the opening angle of the complete dataset which is a result of 1000000 events. On the right side, only the opening angles of the sibling pairs which have one particle with pseudorapidity $\eta > 9.2$ are shown. Here the green region is again the region where the opening angle is big enough for both particles to decay within their respective detectors.

Figure 15 shows the opening angle of the dark photon pairs, compared to their total momenta of the pair. The green area shows the region where the opening angle of the dark photon pair is big enough to allow for the dark photons to travel in the direction of their respective detectors. As can be seen here, only the dark photon pairs with a quite low total momenta have an opening angle which is sufficient for the possible detection of both particles. If the total momentum is too high, both the particles will be forwards boosted, and thus results in a small opening angle.

However, the right most plot of figure 15 shows only the sibling pairs with a particle going in the FASER direction. Here, nearly all the dark photon pairs have too small opening angles for both detectors. Note the difference in axis sizes, the right plot only contains dark photon pairs with high total momenta.

From these plots that were discussed, it can be seen that only very few particles are able to make it to the FASER detector and decay within this volume. In figure 13 only the particles which are within the green area and located along the orange line will decay within FASER. The chances of finding a sibling particle which then ends up decaying inside the ATLAS detector are extremely slim. In order to simulate enough data to be able to compare these results to ATLAS run 4, a lot of simulations have to be done. However, these are very time-consuming. Hence why the probabilistic approach of calculating the probabilities is more viable to finding sibling pairs that will decay within FASER and within ATLAS.

6.2 Probabilistic approach

Now the results from the probabilistic approach can be analysed. As discussed above, it is very hard to get a sufficient number of data using the direct decay output from PYTHIA. Instead of letting PYTHIA do the decay of the dark photons, only the energy of the dark photons and their pseudorapidity is extracted from PYTHIA. From the pseudorapidity of the dark photons, it is possible to determine whether or not the dark photons are travelling in the direction of ATLAS or FASER. From the energy of the dark photon, together with the lifetime which is an input parameter, the probability of a dark photon decaying within a certain volume can be obtained. The probabilities of the dark photons decaying within the FASER and ATLAS detector can be found in figure 16.

From the figure showing the probability of a dark photon to decay within the ATLAS detector, the energy scales on the horizontal axis should be noted. The energy scale is very low. In order to find a higher chance of the dark photons to decay within ATLAS, the energy of the dark photons should be very low. This is due to the longer lifetimes of the dark photons, which are mainly probed for reaching the FASER detector. Since the dark photons have these longer lifetimes, they can easily overshoot the ATLAS detector. The dark photons with low energies are the only dark photons which will not overshoot the ATLAS detector, hence why only these particles have a higher probability to decay within the ATLAS detector. The different coloured lines indicate different values of the pseudorapidity of the dark photons. Dark photons with a pseudorapidity of 0 would travel straight up through the detector, thus only traversing the total height of the detector. However, particles with a higher pseudorapidity will travel more diagonally through the detector, thus traversing more of the detector. Because they travel through more of the detector, they also have a higher chance of decaying within the detector, since they spend more time in it. This effect is most noticeable for dark photons with low energies. Dark photons with a high energy will overshoot the ATLAS detector regardless of their pseudorapidity.

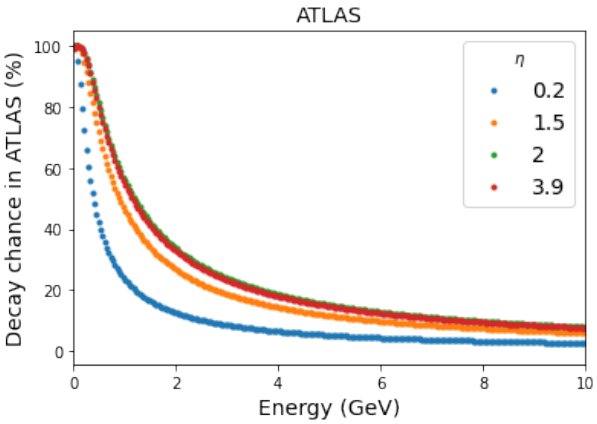

(a) The probability for a dark photon to decay within the ATLAS detector depending on their energy in GeV given in percentage. The colours indicate different pseudorapidity values. Note the small energy scale on the x-axis.

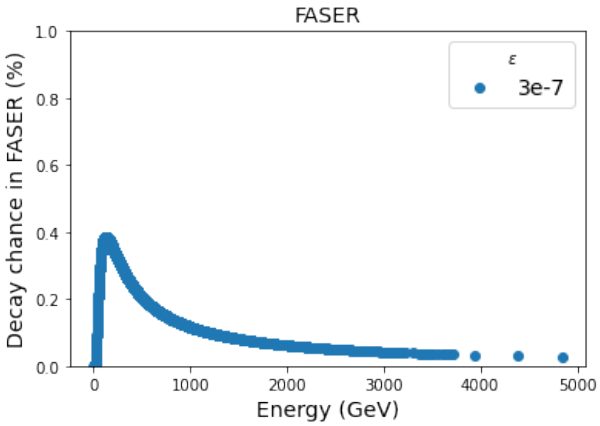

(b) The probability for a dark photon to decay within the FASER detector depending on their energy in GeV. The kinetic mixing parameter ϵ is set to $3*10^{-7}$. The y-axis is scaled to indicate 1%.

Figure 16: The figure on the left shows the probability of a dark photon to decay within the ATLAS detector, depending on their energy and pseudorapidity. Note the low energy scale on the horizontal axis. The different colours indicate different values for the pseudorapidity. The values go up to 4, since the ATLAS inner tracker is sensitive to particles with a pseudorapidity < 4. On the right side the probability of a dark photon decaying within the FASER detector is shown. The kinetic mixing parameter ϵ is set to $3 * 10^{-7}$. Changing the value of the kinetic mixing parameter would also change the location of the optimum. All particles which are shown here have a pseudorapidity > 9.2, otherwise the probability to decay within the FASER detector would be 0. The maximum of the vertical axis is chosen such that the maximum value indicates 1 %. Both figures were made with $\epsilon = 3e - 7$.

On the right side of the figure the probabilities for the dark photons to decay within the FASER detector are shown. Here, an optimum can be seen around an energy of 150 GeV. Dark photons with a lower energy are more likely to decay before reaching the FASER detector. In the same manner, dark photons with a higher energy are more likely to overshoot the FASER detector. The reason for the optimum around 150 GeV is due to the choice of kinetic mixing parameter, since this parameter determines the lifetime of the dark photons. If the lifetime of the dark photons were set to be lower, the dark photons would need more energy to travel the same distance before decaying. However, if the lifetime were longer, the dark photons would need less energy to travel the distance to the FASER detector. From the figure it can also be seen that the maximum probability for dark photons to decay within the FASER detector is 0.004.

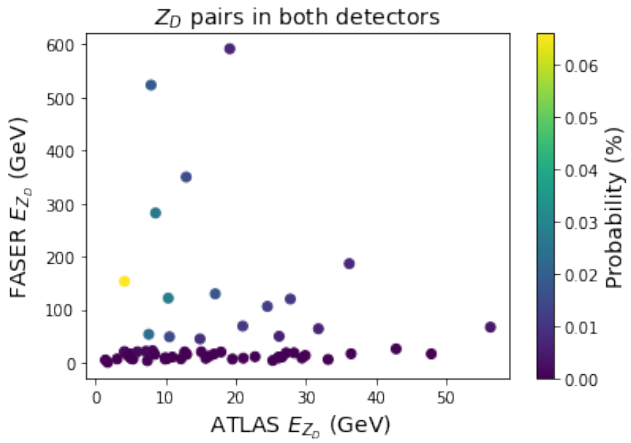

Figure 17: In this figure, each dot represents a dark photon sibling pair. Both of the siblings have to proper pseudorapidity to go in the direction of their respective detector, thus this figure shows all the dark photon pairs from the simulated data that have to potential to decay within both of their detectors. The colour of the dot indicates the combined probability of both dark photons to decay within their detector. On the horizontal axis, the energy of the dark photon sibling which goes in the direction of the ATLAS detector is given in GeV. On the vertical axis, the energy of the FASER going sibling is shown. In total, 130 million events were simulated for the creation of this figure.

Figure 17 shows the probability of dark photon sibling pairs decaying within their respective detectors. In this figure, the energy dependency is shown, with on the horizontal axis the energy of the sibling going to the ATLAS detector, and on the vertical axis the energy of the dark photon sibling going towards the FASER detector. Each dot thus indicates a pair where both dark photons are going in the direction of their respective detectors. Here, it can be seen that, in order for the particles to have a substantial chance to decay within the FASER detector, the energy of the dark photon needs to be higher, i.e. higher than about 40 GeV. This can be seen from the figure, since all the sibling pairs where the FASER going dark photon has an energy lower than 40 GeV are shown to be in the dark purple region, meaning that the probability is very low. The energy where the probability to decay within the FASER detector is optimal is around 150 GeV, as can be seen from the figure 16b, showing the probability for the dark photons to decay within FASER. However, this optimum is dependent on the choice of the kinetic mixing parameter ϵ. Since this parameter alters the lifetime of the dark photons, it also influences where the dark photons will decay. If the energy gets too high, the dark photons will overshoot the FASER detector, and when the energy is too low, they cannot reach the detector. However, overshooting the FASER detector is less of a problem for the total probability of

FASER-ATLAS siblings than undershooting the detector. When the particles have an energy that is too high for the optimum, it is still possible to decay within FASER, only less likely. While it is harder for the dark photons that undershoot the detector to even reach it. This finding is also in accordance with [8].

However, the energies of the ATLAS going particles also play a role in the total probability. In order for the dark photons to have a substantial chance to decay within the ATLAS detector, the energy of the dark photon must not be too high. In figure 17 this can be seen by following the horizontal axis. The dark photons which have a small energy when they go to ATLAS are more lightly coloured, compared to the dark photons which have a higher energy. The dark photons cannot undershoot the ATLAS detector, it is however quite easy for a dark photon to overshoot it. Hence why these small energies are needed. Thus, the optimal case would be to find dark photon siblings where the FASER going sibling has an energy around 150 GeV, and the ATLAS going sibling has a very low energy.

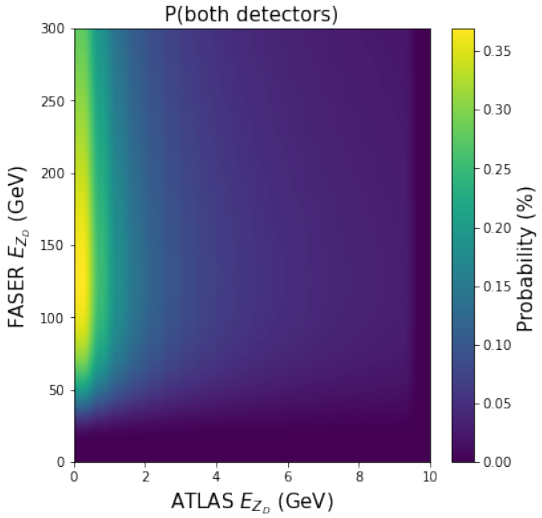

Figure 18: This figure shows the probabilities for the dark photon pairs to decay in both detectors. The figure is made purely of the geometry of the detectors, no simulated data was used for this plot. On the axis, the energy of the dark photons is shown which go to FASER and ATLAS respectively.

Figure 18 shows the same axes as figure 17. The difference between the two figures is that figure 17 shows all the sibling pairs found in the simulations. Figure 18 shows the probability density $\mathcal{P}_{\text{FASER+ATLAS}}$ from equation 56 for all possible combinations of dark photon energies. However, it is not based on any simulated data, it is solely based on the geometry and the calculated probability

of the dark photons to decay within the detectors.

Here the full energy dependence can indeed be seen, not just in the places where particle pairs lie. The ATLAS going dark photon needs to have a low as possible energy, while the FASER going dark photon has the maximal probability to decay within the detector around 150 GeV. Also, the dark photons that undershoot FASER lead to very low combined probabilities, while the dark photons that tends to overshoot it still have a higher probability to decay within in. For dark photons that overshoot ATLAS, the probability drops rapidly.

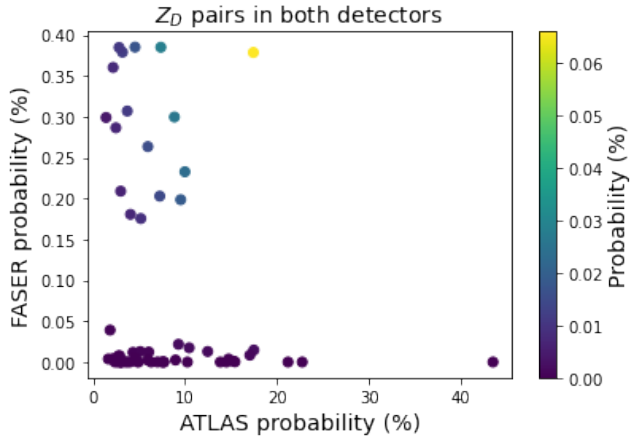

Figure 19: This figure shows the probability of the dark photons to decay within the ATLAS or FASER detector. Each dot again represents a dark photon pair. The colour of the dot indicates the combined probability of the dark photon pair to decay within both detector. The x-axis now shows the probability of the ATLAS going dark photon to decay within the detector. On the y-axis the probability of the sibling dark photon is shown to decay within the FASER detector. Again, 130 million events were simulated for the creation of this figure.

Form figure 19 the probabilities are shown for both sibling particles to decay within their respective detector. Note the difference in scale between the horizontal and vertical axis. The horizontal axis, where the probability for ATLAS is shown, shows the probability in steps of 0.1, leading all the way up to a probability of more than 0.4 for the highest ATLAS probability. However, on the vertical axis where the FASER probability is shown, the scale is considerably different. Here, the steps between indicated points are 0.0005. Thus, the probability of a particle to decay within the FASER detector is considerably smaller than the probability of a particle decaying within the ATLAS detector. This means that the probability for FASER is the limiting factor for the total simultaneous decay probability. This can also be seen from this figure. All the particles which lay in the lower part of the figure, along the horizontal axis, have an extremely

low total probability. Even the particle pair where the ATLAS-going particle has the highest decay probability has a very low total probability. However, when looking at the particle pairs with higher decay probabilities within the FASER detector, the total decay probability also becomes larger. Even though the probability for a decay within the ATLAS detector gets smaller, the total probability does increase compared to the probabilities of the pairs laying near the horizontal axis.

6.3 Scaling to LHC run 4

The plots showing the total number of sibling pairs that are able to reach both the FASER and the ATLAS detector are dependent on the amount of simulated data that I acquired. Since for more data, more sibling pairs could be found in both detectors. In order to make realistic predictions for the LHC based on this, it is more useful to scale the data up to the number of dark photon pairs which will be produced during run 4 of the LHC. This scaling was already discussed in section 5.3. As stated here, the number of dark scalars which are predicted to be found during run 4 can be calculated through knowing the cross section of the process creating the B mesons, the predicted integrated luminosity for run 4, and the branching ratio of the B mesons decaying into dark scalars. The cross section for the B meson production can be retrieved from the PYTHIA simulations. Here it is important to look at the cross sections without the pT-cuts implemented in the simulations. The found cross section is $\sigma_B = 3.83 * 10^{11}$ fb. The integrated luminosity, which is predicted for run 4 of the LHC, is $\mathcal{L}_{int} = 3000$ fb^{-1} [23]. This leads to finding $1 * 10^{15}$ B mesons during run 4. In order to find the number of dark scalars, and thus the number of dark photon pairs which will be produced from these B mesons, it needs to be multiplied by the branching ratio of the B mesons going to a dark scalar and Kaon. From table 2, the branching ratios can be seen. The Higgs-dark scalar mixing angle is given as $\theta_\phi = 0.008$, leading to 61614352871 dark scalars found in run 4, while in the simulations 102007812 dark scalars were produced. This means that the ratio of dark scalars in run 4 compared to the number of dark scalars found in the simulations is 604. The number of dark scalars which are produced during run 4 can now be compared to the number of dark scalars which are simulated by PYTHIA. From this, a scaling factor can be determined. Now the data from PYTHIA can be scaled up to meet the run 4 data.

After scaling to run 4 data, the number of dark photon pairs predicted to be in the direction of both detectors is 37925 for LHC run 4. However, the probability of finding these dark photon pairs in both detectors does remain very low. Also, this scaling is affected by statistical uncertainties, since there are not a lot of dark photon pairs found that decay within both detectors.

7 Discussion

From the results of Method 1, it can thus be seen that the number of dark photons which are produced in the FASER detector is very small. Even when the kinetic mixing parameter ϵ is specifically chosen so that the number of dark photons is optimized for FASER, and the pT-cut is installed on the simulations, the number of dark photons found in FASER remains very low. This can also be seen when looking at both figure 14 and 15. From figure 15, it can be seen that the total momentum should be lower than about 1 GeV in order to have a sufficient opening angle. However, from figure 14, it is seen that the dark photons with a high enough momentum make it to the FASER detector.

From the results of the probabilistic approach, it can be seen that it is not impossible to find particle pairs where one goes to the ATLAS detector and one goes to the FASER detector. However, the chances of detecting these pairs are very slim, as can be seen from figure 17. Not a lot of dark photon pairs making it to their detectors were found in the simulated data, and of the pairs that do make it to both detectors, the probability of finding them is very low. This low probability is mainly due to the geometry of the detectors, especially the FASER detector. Since this detector is such a small detector, it needs both a very high pseudorapidity to even make it to the detector, and it has a very limited decay volume for the dark photons to decay into, especially when comparing this to the distance that the dark photons have to traverse to get there. Due to this geometry, the maximum probability of finding a dark photon here is thus only 0.004. On top of this small probability, also the probability of the ATLAS detector will reduce the total probability. Since the dark photons are probed for the decay within FASER, they will very likely overshoot the ATLAS detector, leading to probabilities lower or around 0.1, as can be seen in figure 19.

The number of dark photon pairs which is found is also low, compared to the total number of dark photons which were produced. Of all of the dark photons which were produced in the simulations, only a fraction of 0.0001 dark photons travel in the direction of the FASER detector. Thus the need for the dark photons to travel in the direction of FASER already reduces the number of dark photons which I am interested in by 0.01%. Next to this, of the dark photons which do travel in the direction of FASER, only a fraction of 0.004 of the dark photons has a sibling which is travelling in the direction of ATLAS. Thus the chance of finding a sibling which is travelling to ATLAS if its sibling does go to the FASER detector is 0.4%.

The scaling of the dark scalars to run 4 leads to finding 37925 dark photon pairs, of which both dark photons travel in the direction of the respective detectors. However, the scaling of the dark photons to run 4 data does depend on the beginning sample size, thus on the number of dark photon pairs found in the simulated data. A statistical uncertainty in predicted dark photon pairs of 36% can be found when comparing how sections of the simulated dataset

scale compared to the total simulated dataset. In order to find this difference, the total dataset was divided into 5 equal sections, of which the difference with respect to one fifth of the dataset was determined.

8 Conclusion

In this thesis, the dark photon benchmark model has been discussed in detail. The relevant parameters have been discussed, and with this choice of parameters, simulations have been made. The data that was produced as a result of these simulations has been analysed to find possible dark photon pairs which both travel to the FASER and ATLAS detectors respectively. Also, the probability of having both these dark photons decay within their respective detectors has been determined.

From the scaled LHC run 4 data it is thus predicted to find 37925 dark photon pairs in both the FASER and the ATLAS detector. However, this is for a specific set of parameters. Also, the probabilities of finding these dark photon pairs in these detectors are extremely slim. For this choice of parameters, the highest probability will be found for a dark photon pair where the ATLAS-going dark photon has an energy < 10 GeV, and the FASER-going sibling has an energy of 150 GeV. In this case the probability of finding the dark photon pair would be optimal. But even this optimal probability will be highly suppressed by the probability of the dark photon decaying in FASER.

In summary, the necessity to find a dark photon in the direction of FASER already reduces the possible number of dark photon pairs to 0.01%. Next to this, the probability for the other dark photon to fly in the direction of the ATLAS detector on top of the FASER detector reduces this by 0.4%. Thus, only through the geometry of the detectors, 5 orders of magnitude of the produced dark photon pairs are lost.

Next, also the probability of finding both particles in the detector is very slim. The FASER detector already suppresses it to 0.4 percent. On top of that, the ATLAS detector will also suppress the total probability. Only for dark photons with an energy lower than about 10 GeV will the probability be higher than 10%, depending on the pseudorapidity of the dark photon.

When scaling the number of dark photon pairs, of which both particles travel to their respective detector, up to match run 4 data, 37925 dark photon pairs are predicted. However, in a data sample of 130 million, this number does fluctuate due to the size of the simulated data, up to 36%. Also, the probability of both of the dark photons actually decaying within their respective detectors is still very low.

Thus, is it useful to link the FASER and the ATLAS detector? It is not impossible for a dark photon pair to decay both within the FASER and ATLAS detectors respectively. However, the probability of it occurring during LHC run 4 is very slim.

9 Outlook

In this thesis, the parameters which play a role in the model were specifically set. However, a change in parameter choice could also lead to different behaviour of the dark photons. It could be insightful to see how these different parameter choices affect the model. Since this could affect the number of dark photon pairs going in the detectors, and the probabilities of actually finding them.

Next, the probability of finding the pairs could be increased when looking at the Kaon from $B \to K\phi$ and one dark photon in FASER, instead of looking at two dark photons. All kaons, with appropriate pseudorapidities, can decay within the ATLAS detector. This would result in a much higher probability of finding a particle pair, since ATLAS would no longer suppress it. However, distinguishing the signal Kaons might still be a problem, since Kaons are produced in a lot of processes within ATLAS, leading to high backgrounds.

Lastly, there is also a FASER upgrade suggested. FASER-2 would have a volume about 600 times greater than the volume of the current FASER detector [24]. This could significantly improve the number of dark photon pairs which travel to both detectors, since this would mean that the opening angle for both detectors is smaller. The upgraded detector will not only have a bigger radius, but also have a longer decay volume. Because of this, the probability for dark photons to decay within FASER-2 and the reach in dark photon lifetime also increases compared to the current FASER detector.

Appendix

A Scalar mixing angle

In order to determine experimental bounds on the Standard Model Higgs-dark scalar mixing angle, I performed the following calculations. The scalar mixing angle can be constrained through the invisible decays of the Standard Model Higgs boson. The relation between the invisible branching ratio and the mixing angle can be found in [25] figure 2. This same figure is here shown as figure 20.

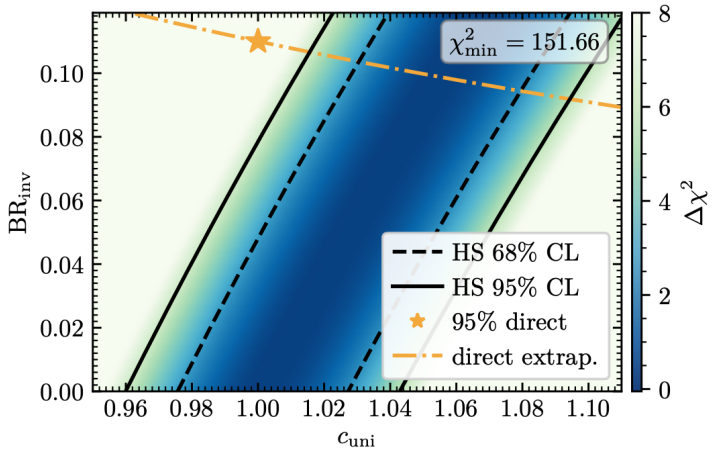

Figure 20: This figure shows the relation between the invisible branching ratio BR_{inv} of the Standard Model Higgs, and bounds on c_{uni}, which is the cosine of the mixing angle θ_ϕ. The figure can be found in [25] figure 2.

In order to find the invisible branching ratio of the Standard Model Higgs of this benchmark model, the following equation has been used

$$BR(h \to inv; \theta_\phi) = \frac{\Gamma_{h\to Z_D Z_D}(1-\mathcal{P}_{det})^2}{\cos^2\theta_\phi \Gamma_{SM} + \Gamma_{h\to Z_D Z_D}(1-\mathcal{P}_{det})^2}. \tag{57}$$

Here, the decay width of the Standard Model Higgs going to a dark photon pair is described as:

$$\Gamma_{h\to Z_D Z_D} = \sin^2\theta * \Gamma_{\phi\to Z_D Z_D}(m_\phi \to m_h). \tag{58}$$

This thus represents the decay width of the invisible Higgs decays of this model provided that the dark photons are invisible to the ATLAS and CMS detectors. In equation 57, $\mathcal{P}_{det}$ refers to the probability of finding the decay products of the dark photon in the detector. Thus, the $1-\mathcal{P}_{det}$ refers to the probability of not finding the particle in the detector. This term is squared,

since the decay results in two dark photons. $\mathcal{P}_{det}$ can be calculated using equation 55. Here, r_{max} is chosen to be 1 meter. This rough estimated of the outer detector boundaries can be used due to the high momentum of the dark photons [26]. They are very likely to overshoot the ATLAS detector. The parameter r_{max} does not change a lot to this result, it will only result in a change of decimals for the resulting bound on the scalar mixing angle. The same goes for the shape of the detector. Here, the detector is assumed to be spherically symmetric, which is of course not the real case.

Equation 57 will thus result in an expression for the invisible branching ratio as a function of the mixing angle θ_ϕ. In order to find the proper value of the invisible branching ratio, this has to be compared to the following experimental bound [25].

$$BR_{inv} < 0.078 \left(1 - \left(\frac{\theta}{0.285}\right)^2\right) \tag{59}$$

After inserting BR_{inv} from equation 57 into 59, the experimental bound on θ_ϕ can be determined. For this model, the invisible branching ratio that is found is 0.079. This results in a Standard Model Higgs-dark scalar mixing angle $\theta_\phi \leq 0.008$. As can be seen from equation 59, the results found are the upper value for the mixing angle, since equation 59 is an inequality.

B Dark photon couplings to fermions.

In this appendix, the coupling constants for the dark photon coupling to fermions will be determined. Here, the conventions from Denner [27] will be used:

$$D_\mu = \partial_\mu - igI_w^a W_\mu^a + ig'\frac{Y_w}{2}B_\mu. \tag{60}$$

The Lagrangian can be written as

$$\begin{aligned}\mathcal{L}_{ew} = &\sum_A \bar{Q}'_{A_L} i\gamma^\mu \left[-igI_w^a W_\mu^a + ig'\frac{Y_w}{2}\tilde{B}_\mu\right] Q'_{A_L} \\ &+ \sum \left(\bar{u}'_{A_R} i\gamma^\mu \left[ig'\frac{Y_w}{2}\tilde{B}_\mu\right] u'_{A_R} + \bar{d}'_{A_R}\left[ig'\frac{Y_w}{2}\tilde{B}_\mu\right] d'_{A_R}\right).\end{aligned} \tag{61}$$

Here, the tilde indicates that the fields are not yet mass eigenstates. The neutral current is thus

$$NC = -\sum_q \bar{\psi}_q\gamma^\mu \left[-P_L g I_w^3 W_\mu^3 + P_L g'\frac{Y_w}{2}\tilde{B}_\mu + P_R g'\frac{Y_w}{2}\tilde{B}_\mu\right]\psi_q. \tag{62}$$

Now with the use of equation 19 the $\tilde{B}$ can be rewritten in terms of Z_D and B, the fields after the shift, but before the diagonalization to mass eigenstates.

$$NC = -\sum_q \bar{\psi}_q\gamma^\mu \left[-P_L g I_w^3 W_\mu^3 + P_L g'\frac{Y_w}{2}\left(\frac{\epsilon}{c_w}Z_{D_\mu} + B_\mu\right) + P_R g'\frac{Y_w}{2}\left(\frac{\epsilon}{c_w}Z_{D_\mu} + B_\mu\right)\right]\psi_q. \tag{63}$$

Now write the W_μ^3 and B_μ as linear combinations using the following relations

$$\begin{aligned} W_\mu^3 &= c_w Z_\mu - s_w A_\mu \\ B_\mu &= s_w Z_\mu + c_w A_\mu \end{aligned}. \tag{64}$$

So the part containing the Z and Z_D gives

$$
\begin{aligned}
\mathcal{L} = &-\sum_q \bar{\psi}_q \gamma^\mu \left[-P_L g c_w I_3 Z_\mu + P_L g' \frac{Y_{w_L}}{2} \frac{\epsilon}{c_w} Z_{D_\mu} + P_L g' \frac{Y_{w_L}}{2} s_w Z_\mu \right. \\
&\left. + P_R g' \frac{Y_{w_R}}{2} \frac{\epsilon}{c_w} Z_{D_\mu} + P_R g' \frac{Y_{w_R}}{2} s_w Z_\mu \right] \psi_q \\
= &-\sum_q \bar{\psi}_q \gamma^\mu Z_{D_\mu} \left[P_L g' \frac{Y_{w_L}}{2} \frac{\epsilon}{c_w} + P_R g' \frac{Y_{w_R}}{2} \frac{\epsilon}{c_w} \right] \psi_q \\
&-\sum_q \bar{\psi}_q \gamma^\mu Z_\mu \left[-P_L g c_w I_3 + P_L g' \frac{Y_{w_L}}{2} s_w + P_R g' \frac{Y_{w_R}}{2} s_w \right] \psi_q \\
= &-\sum_q \bar{\psi}_q \gamma^\mu Z_{D_\mu} \frac{1}{c_w} \left[P_L g s_w \frac{Y_{w_L}}{2} \frac{\epsilon}{c_w} + P_R g s_w \frac{Y_{w_R}}{2} \frac{\epsilon}{c_w} \right] \psi_q \\
&-\sum_q \bar{\psi}_q \gamma^\mu Z_\mu \frac{1}{c_w} \left[-P_L g c_w^2 I_3 + P_L g \frac{Y_{w_L}}{2} s_w^2 + P_R g \frac{Y_{w_R}}{2} s_w^2 \right] \psi_q \\
= &-\sum_q \bar{\psi}_q \gamma^\mu Z_{D_\mu} \frac{g}{c_w} \left[P_L s_w \frac{Y_{w_L}}{2} \frac{\epsilon}{c_w} + P_R s_w \frac{Y_{w_R}}{2} \frac{\epsilon}{c_w} \right] \psi_q \\
&-\sum_q \bar{\psi}_q \gamma^\mu Z_\mu \frac{g}{c_w} \left[-P_L \left(c_w^2 I_3 - \frac{Y_{w_L}}{2} s_w^2 \right) + P_R \frac{Y_{w_R}}{2} s_w^2 \right] \psi_q .
\end{aligned}
\tag{65}
$$

Now use equation 26 to rewrite to the mass eigenstates.

$$
\begin{aligned}
\mathcal{L} = &-\sum_q \frac{g}{c_w} \bar{\psi}_q \gamma^\mu \hat{Z}_{D_\mu} \cos\theta_d \left[P_L s_w \frac{Y_w}{2} \frac{\epsilon}{c_w} + P_R s_w \frac{Y_R}{2} \frac{\epsilon}{c_w} \right] \psi_q \\
&+ \sum \frac{g}{c_w} \bar{\psi} \gamma^\mu \hat{Z}_{D_\mu} \sin\theta_d \left[-P_L \left(c_w^2 I_3 - s_w^2 \frac{Y_w}{2} \right) + P_R s_w^2 \frac{Y_w}{2} \right] \psi_q .
\end{aligned}
\tag{66}
$$

Thus the left- and right-handed coupling constants of the dark photons are

$$
g_L = \frac{g}{c_w} \left[-\cos\theta_d s_w \frac{Y_{w_L}}{2} \frac{\epsilon}{c_w} - \sin\theta_d \left(c_w^2 I_3 - s_w^2 \frac{Y_{w_L}}{2} \right) \right] \tag{67}
$$

$$
g_R = \frac{g}{c_w} \left[-\cos\theta_d s_w \frac{Y_{w_R}}{2} \frac{\epsilon}{c_w} + \sin\theta_d s_w^2 \frac{Y_{w_R}}{2} \right] . \tag{68}
$$

These also agree with [10].

References

[1] *Detector & Technology*. URL: %7Bhttps://atlas.cern/Discover/Detector%7D.

[2] Katherine Freese. "Status of dark matter in the universe". In: *International Journal of Modern Physics D* 26.06 (Mar. 2017), p. 1730012. ISSN: 1793-6594. DOI: 10.1142/s0218271817300129. URL: http://dx.doi.org/10.1142/S0218271817300129.

[3] David Curtin et al. "Exotic decays of the 125 GeV Higgs boson". In: *Physical Review D* 90.7 (Oct. 2014). ISSN: 1550-2368. DOI: 10.1103/physrevd.90.075004. URL: http://dx.doi.org/10.1103/PhysRevD.90.075004.

[4] Hooman Davoudiasl, Hye-Sung Lee, and William J. Marciano. ""Dark" Z implications for parity violation, rare meson decays, and Higgs physics". In: *Physical Review D* 85.11 (June 2012). ISSN: 1550-2368. DOI: 10.1103/physrevd.85.115019. URL: http://dx.doi.org/10.1103/PhysRevD.85.115019.

[5] David Curtin et al. "Illuminating dark photons with high-energy colliders". In: *Journal of High Energy Physics* 2015.2 (Feb. 2015). ISSN: 1029-8479. DOI: 10.1007/jhep02(2015)157. URL: http://dx.doi.org/10.1007/JHEP02(2015)157.

[6] S. Navas et al. "Review of particle physics". In: *Phys. Rev. D* 110.3 (2024), p. 030001. DOI: 10.1103/PhysRevD.110.030001.

[7] Shrihari Gopalakrishna, Sunghoon Jung, and James D. Wells. "Higgs boson decays to four fermions through an Abelian hidden sector". In: *Physical Review D* 78.5 (Sept. 2008). ISSN: 1550-2368. DOI: 10.1103/physrevd.78.055002. URL: http://dx.doi.org/10.1103/PhysRevD.78.055002.

[8] Jonathan L. Feng et al. "Dark Higgs bosons at the ForwArd Search ExpeRiment". In: *Physical Review D* 97.5 (Mar. 2018). ISSN: 2470-0029. DOI: 10.1103/physrevd.97.055034. URL: http://dx.doi.org/10.1103/PhysRevD.97.055034.

[9] Kingman Cheung et al. *Probing dark photons from a light scalar at Belle II*. 2024. arXiv: 2401.03168 [hep-ph]. URL: https://arxiv.org/abs/2401.03168.

[10] María Cepeda et al. "Exotic Higgs Decays". In: *Annual Review of Nuclear and Particle Science* 72.1 (Sept. 2022), pp. 119–149. ISSN: 1545-4134. DOI: 10.1146/annurev-nucl-102319-024147. URL: http://dx.doi.org/10.1146/annurev-nucl-102319-024147.

[11] Takeshi Araki et al. "Dark photon from light scalar boson decays at FASER". In: *JHEP* 03 (2021). [Erratum: JHEP 06, 087 (2021)], p. 072. DOI: 10.1007/JHEP03(2021)072. arXiv: 2008.12765 [hep-ph].

[12] Luca Buonocore et al. "Predictions for neutrinos and new physics from forward heavy hadron production at the LHC". In: *The European Physical Journal C* 84.4 (Apr. 2024). ISSN: 1434-6052. DOI: 10.1140/epjc/s10052-024-12726-5. URL: http://dx.doi.org/10.1140/epjc/s10052-024-12726-5.

[13] Martin Wolfgang Winkler. "Decay and detection of a light scalar boson mixing with the Higgs boson". In: *Physical Review D* 99.1 (Jan. 2019). ISSN: 2470-0029. DOI: 10.1103/physrevd.99.015018. URL: http://dx.doi.org/10.1103/PhysRevD.99.015018.

[14] Iryna Boiarska et al. "Phenomenology of GeV-scale scalar portal". In: *Journal of High Energy Physics* 2019.11 (Nov. 2019). ISSN: 1029-8479. DOI: 10.1007/jhep11(2019)162. URL: http://dx.doi.org/10.1007/JHEP11(2019)162.

[15] Daniel Aloni, Yotam Soreq, and Mike Williams. "Coupling QCD-Scale Axionlike Particles to Gluons". In: *Physical Review Letters* 123.3 (July 2019). ISSN: 1079-7114. DOI: 10.1103/physrevlett.123.031803. URL: http://dx.doi.org/10.1103/PhysRevLett.123.031803.

[16] O. Aad Zormpa et al. "The ATLAS experiment at the CERN Large Hadron Collider: a description of the detector configuration for Run 3". In: *Journal of Instrumentation* 19.05 (May 2024), P05063. ISSN: 1748-0221. DOI: 10.1088/1748-0221/19/05/p05063. URL: http://dx.doi.org/10.1088/1748-0221/19/05/P05063.

[17] Rende Steerenberg. *Accelerator report: LHC run 3 achieves record-breaking integrated luminosity*. Sept. 2024. URL: https://home.cern/news/news/accelerators/accelerator-report-lhc-run-3-achieves-record-breaking-integrated-luminosity.

[18] O. Aberle, M. Zobov, and I. Zurbano Fernandez. *High-Luminosity Large Hadron Collider (HL-LHC): Technical design report*. CERN Yellow Reports: Monographs. Geneva: CERN, 2020. DOI: 10.23731/CYRM-2020-0010. URL: https://cds.cern.ch/record/2749422.

[19] *Technical Design Report for the ATLAS Inner Tracker Pixel Detector*. Tech. rep. Geneva: CERN, 2017. DOI: 10.17181/CERN.FOZZ.ZP3Q. URL: https://cds.cern.ch/record/2285585.

[20] FASER Collaboration et al. *Technical Proposal for FASER: ForwArd Search ExpeRiment at the LHC*. 2018. arXiv: 1812.09139 [physics.ins-det]. URL: https://arxiv.org/abs/1812.09139.

[21] Christian Bierlich et al. *A comprehensive guide to the physics and usage of PYTHIA 8.3*. 2022. arXiv: 2203.11601 [hep-ph]. URL: https://arxiv.org/abs/2203.11601.

[22] Torbjörn Sjöstrand et al. "An introduction to PYTHIA 8.2". In: *Computer Physics Communications* 191 (June 2015), pp. 159–177. ISSN: 0010-4655. DOI: 10.1016/j.cpc.2015.01.024. URL: http://dx.doi.org/10.1016/j.cpc.2015.01.024.

[23] R De Maria et al. "High Luminosity LHC optics scenarios for Run 4". In: *JACoW IPAC* 2023 (2023), MOPL034. DOI: 10.18429/JACoW-IPAC2023-MOPL034. URL: https://cds.cern.ch/record/2886006.

[24] Olivier Salin et al. "FASER2: Detector Design and Performance". In: (2025). URL: https://cds.cern.ch/record/2927003.

[25] Thomas Biekötter and Mathias Pierre. "Higgs-boson visible and invisible constraints on hidden sectors". In: *The European Physical Journal C* 82.11 (Nov. 2022). ISSN: 1434-6052. DOI: 10.1140/epjc/s10052-022-10990-x. URL: http://dx.doi.org/10.1140/epjc/s10052-022-10990-x.

[26] The Group et al. "First look at the physics case of TLEP". In: *Journal of High Energy Physics* 2014 (Jan. 2014), p. 164. DOI: 10.1007/JHEP01%282014%29164.

[27] Ansgar Denner. *Techniques for the calculation of electroweak radiative corrections at the one-loop level and results for W-physics at LEP200*. 2007. arXiv: 0709.1075 [hep-ph]. URL: https://arxiv.org/abs/0709.1075.